HALLOYSITE CONTAINING POLYURETHANE FOAMS AS INSULATION MATERIALS WITH ENHANCED FLAME RETARDANCE

by

DENİZ ANIL

Submitted to the Graduate School of Engineering and Natural Sciences
in partial fulfillment of
the requirements for the degree of
Master of Science

SABANCI UNIVERSITY
July 2019

HALLOYSITE CONTAINING POLYURETHANE FOAMS AS INSULATION MATERIALS WITH ENHANCED FLAME RETARDANCE

APPROVED BY:

Asst. Prof. Dr. Serkan Ünal...
    (Thesis Supervisor)

Prof. Dr. Kürşat Şendur...
    (Thesis Co-Supervisor)
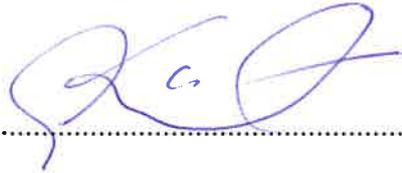
Prof. Dr. Yusuf Menceloğlu..
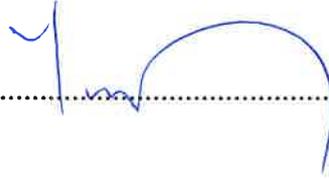
Asst. Prof. Dr. Bekir Dizman..

Assoc. Prof. Dr. Engin Burgaz..
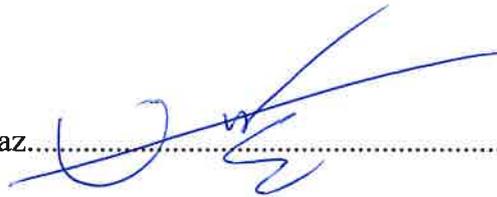
DATE OF APPROVAL: 16/07/2019

Halloysite Containing Polyurethane Foams as Insulation Materials with Enhanced Flame Retardance

DENİZ ANIL

M.Sc. Thesis, July 2019

Thesis Advisors: Asst. Prof. Dr. Serkan Ünal and Prof. Dr. Kürşat Şendur

Keywords: Rigid Polyurethane Foams, Halloysite Nanotubes, Thermal Conductivity, Flame Retardancy

ABSTRACT

Rigid polyurethane foams (RPUFs) are one of the high-performance insulation materials preferred due to their superior thermal insulation properties, good chemical durability, high mechanical strength and easy processability. Nevertheless, low thermal stability and high flammability of RPUFs is a critical concern in insulation applications. Conventionally, flame retardants (FRs) are used to overcome these problems. However, typically high amounts of environmentally unfriendly FR agents are added into RPUFs to provide flame retardancy. Such FR agents can be partially replaced by alternative additives to provide safer flame retardancy. Halloysite nanotubes (HNT) are low cost, abundant clay minerals, standing as unique, environmentally friendly alternatives to numerous nanofillers. During burning, HNTs are expected to reinforce the char layer and entrap flammable decomposition products.

They contribute to the formation of smaller foam cells, which reduce thermal conductivity. Yet, it is critical to obtain a homogeneous dispersion of HNTs in the RPUF matrix.

This thesis focuses on the incorporation of HNTs into RPUFs and understanding of their thermal insulation and flammability behavior. HNTs that were untreated, sonicated, chemically functionalized and FR-loaded were incorporated into RPUF formulations. The morphology, thermal conductivity and flammability behavior of resulting nanocomposites were studied extensively. Halogenated FR content in the RPUF formulation was replaced with FR-loaded HNTs with much lower FR content, which resulted in nanocomposites with comparable total heat release and peak heat release rates to existing commercially available RPUFs.

Halloysite Containing Polyurethane Foams as Insulation Materials with Enhanced Flame Retardance

DENİZ ANIL

Yüksek Lisans Tezi, Temmuz 2019

Tez Danışmanları: Dr. Öğr. Üyesi Serkan Ünal ve Prof. Dr. Kürşat Şendur

Anahtar Kelimeler: Rijit Poliüretan Köpük, Halloysit Nanotüp, Termal İletkenlik, Alev Geciktiricilik

ÖZET

Sert poliüretan köpük, üstün ısı yalıtım özelliği, yüksek kimyasal ve mekanik dayanıklılığı ve kolay işlenebilirliği nedeniyle tercih edilen yüksek performanslı yalıtım malzemelerinden biridir. Bununla birlikte, bu köpüklerin düşük termal stabiliteleri ve yüksek yanıcılığı yalıtım uygulamalarında önemli bir sorundur. Endüstriyel olarak, bu problemlerin üstesinden gelmek için alev geciktiriciler kullanılmaktadır. Ancak bu kimyasallar çoğunlukla hem çevre hem de insan sağlığı için zararlıdır ve kabul edilebilir alev geciktiriciliği sağlayabilmeleri için polimerlere yüksek miktarlarda eklenmeleri gerekmektedir. Daha iyi ve güvenli alev geciktirme etkisi sağlamak için alev geciktiriciler kısmen alternatif katkı maddeleri ile birleştirilebilir. Halloysit nanotüp (HNT), düşük maliyetli, doğada bol bulunan kil temelli bir mineraldir ve özgün yapısı sayesinde birçok sentetik katkı maddesine çevre dostu bir alternatiftir. Yanma sırasında, HNTler malzeme yüzeyinde oluşan kömür tabakasını

iii

güçlendirebilir ve polimerin oluşturduğu yanıcı bozunma ürünlerini lümeninde tutabilir. Isı yalıtımı açısından, termal iletkenliği azaltmak için köpük matrisinde daha küçük hücrelerin oluşumuna katkıda bulunabilir. Diğer kil temelli malzemelerde olduğu gibi, HNTlerin polimer matrisindeki dağılımı ideal bir yapı elde etmek açısından oldukça kritiktir.

Bu tez HNT'lerin rijit poliretan köpüklere eklenmesine ve bu nanokompozitlerin termal yalıtım ve yanmazlık davranışlarının incelenmesine odaklanmaktadır. İşlemden geçmemiş, ultrasonikasyona tabii tutulmuş, kimyasal olarak fonksiyonlandırılmış ve alev geciktirici yüklenmiş HNT'ler köpük formülasyonlarına eklenmiştir. Bu nanokompozitlerin morfolojisi, termal iletkenliği ve yanma davranışı detaylı şekilde çalışılmıştır. Köpük formülasyonundaki halojenli alev geciktirici içeriği kısmen alev geciktirici yüklenmiş HNT'ler ile değiştirilmiş ve üretilen nanokompozit köpüklerin daha yüksek halojenli alev geciktirici içeriğine sahip mevcut ticari köpüklerinkiyle karşılaştırılabilir toplam ısı salımı ve tepe ısı salımı değerlerine sahip olduğu görülmüştür.

For only the good doubt their own goodness, which is what makes them good in the first place. The bad know they are good, but the good know nothing. They spend their lives forgiving others, but they can't forgive themselves.

Paul Auster

Anneme ve babama…

ACKNOWLEDGEMENTS

Finally, I would like to thank my mother and my father for always supporting and encouraging me. I also appreciate my father's help in this work, with his perspective, enthusiasm and love of science. This would not be possible without you both.

Table of Contents

List of Figures

List of Tables

List of Equations

List of Abbreviations

APP	Ammonium polyphosphate
APTES	γ-aminopropyl triethoxysilane
CNT	Carbon nanotube
DMMP	Dimethyl methyl phosphonate
D_s max	Maximum specific optical density
FPUF	Flexible polyurethane foam
FR	Flame retardant
FT-IR	Fourier transform infrared spectroscopy
HNT	Halloysite nanotube
HRR	Heat release rate
IFR	Intumescent flame retardant
IPTES	3-isocyanatopropyl triethoxysilane
LOI	Limiting oxygen index
MLR	Mass loss rate
MMT	Montmorillonite
pHRR	Peak heat release rate
PMDI	Polymeric methylene diphenyl diisocyanate
PPO	Polypropylene oxide
PU	Polyurethane
RPUF	Rigid polyurethane foam
SEA	Specific extinction area
SEM	Scanning electron microscopy
SPR	Smoke production rate

TCPP	Tris(1-chloro-2-propyl) phosphate
TGA	Thermogravimetric analysis
THR	Total heat released
TSR	Total smoke released
TTI	Time to ignition

Chapter 1

1. Introduction

1.1. Overview

Following the research of Wurtz showing the synthesis of isocyanate and formation of urethane groups, polyurethanes (PUs) were discovered by Otto Bayer and coworkers in 1937. Since then, there are PU products available for almost any purpose. They are used as elastomers, foams, coatings, adhesives and sealants, responding to all types of needs. With global production reaching 18 million tonnes in 2016, PUs were ranked 6th among all polymers in terms of annual production [1]. Today, rigid polyurethane foams (RPUFs) and flexible polyurethane foams (FPUFs) constitute a big share of the PU market.
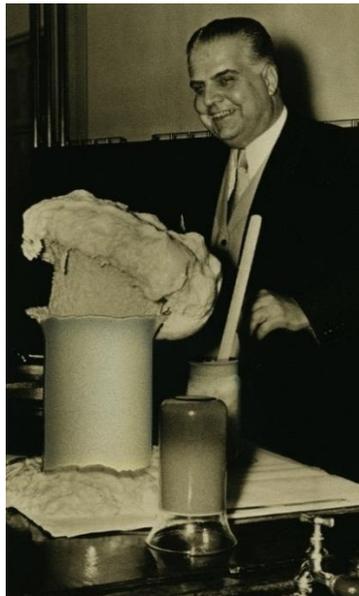
Figure 1. Otto Bayer in 1952 [2]

RPUFs are used mainly for insulation purposes in constructions, pipes and several appliance products and as air-barrier insulating sealants. They have high mechanical strength and chemical durability, easy processability and remarkable thermal insulation capability, in addition to their versatility in chemistry [3]. However, RPUFs have low thermal stability, they are highly flammable and produce significant amounts of toxic gases and smoke during burning. Conventionally, flame retardants (FRs) are added to RPUF formulations to enhance flammability issues. These additives take a role in the formation of a char layer on the burning polymer surface and can quench flammable radicals released from the polymer and act as heat sinks [4]. These effects are observable at different degrees depending on the chemistry of the FRs used. However, commercially and conventionally used FRs in the past and present generally need to be added in high amounts to obtain acceptable flame retardancy. They also put both human health and environment at risk due to their toxic nature. Newer technologies seek harmless FR systems. The chemistry behind the development of FRs for RPUFs is considerably flexible and these formulations can become even more efficient by the use of nanoparticles. FR amount can be partially replaced by particulate additives to provide better flame retardancy [5].

Halloysite nanotubes (HNTs) are abundantly available clay materials. They are environmentally friendly and serve as cheap options for other tubular nanoparticles. HNTs possess an elongated, tubular shape, like a rolled sheet, where the outer surface is composed of alumina and inner surface is composed of silanol groups. The unique chemical composition and shape of HNTs make them ideal candidates for utilization in a variety of applications. Their inner, interlayer and outer surface can be functionalized through existing hydroxyl groups. Such functionalizations are used for making the hydrophilic HNTs more compatible with polymer matrices, as well as enhancing the dispersion of the particles. Certainly, homogeneous dispersion of nanoparticles in the polymer matrix is critical for the final properties of the nanocomposite. Additionally, HNT lumens can be filled with different agents, such as anti-bacterials and FRs, and controlled release of these can be provided in a respective application [6]. For flame retardant applications, in case of fire, HNTs help by reinforcing the char layer formed on the burning surface, while entrapping decomposition products of the polymer in their lumen. They can also release their structural water at high temperatures (above 400°C), which could provide a cooling effect [7].

1.2. Aim and Objective

Even though RPUFs are very good thermal insulators, they are highly flammable. Nevertheless, both of these properties can be enhanced through the proper incorporation of nanoparticles into the foam matrix. This thesis aims to enhance or maintain the original thermal insulation performance of RPUFs while improving their flammability behavior using HNTs. HNTs are expected to play a role not only in reducing the cell size of RPUFs, which positively contributes to the decreament of thermal conductivity but also improving the flame retardancy by reinforcing the char layer and releasing inner structural water during the burning process of the foam.

1.3. Main Contributions

This thesis specifically focuses on the thermal conductivity and flammability of RPUFs currently used in the industry. It is one of the very few studies concerned with RPUF-HNT nanocomposites, however it is the first study in the literature reporting the flammability of these nanocomposites in detail.

It is also important to note that this thesis critically addresses the dispersion and compatibility of HNTs with the foam matrix by their surface modification with polypropylene oxide based oligomers covalently attached with the aid of a silane coupling agent, which has not been reported in the literature for this purpose previously. Furthermore, the effect of the incorporation of HNTs into halogenated FR containing RPUF formulations has been investigated in an effort to decrease or eliminate the halogenated FR amount used in these formulations by loading HNTs with FR agents.

1.4. Thesis Outline

Remainder of Chapter 1 provides detailed background information about RPUFs and HNTs. In Chapter 2, experimental steps and procedures for the processing of HNTs, synthetic routes and foam production are explained in detail. Methods to characterize raw materials, intermediate products and final foam structures are also described. In Chapter 3, experimental and theoretical studies related to the thermal conductivity of foams are presented. Introduction to this chapter covers the evolution of thermal insulation performance in RPUFs

with a theoretical background. It also touches on the possible effects of the nanoparticles in such systems. In Chapter 4, firstly a detailed literature review concerning flame retardancy of RPUFs and HNTs is provided. Reasons behind high flammability of RPUFs and solutions reported in the literature until now are explained. Finally, detailed studies and results of advanced flammability tests are presented for RPUF-HNT foams that were prepared by the incorporation of HNTs, PPO-functionalized HNTs, HNTs and a halogenated FR agent individually, and finally HNTs loaded with the halogenated FR agent, later in this chapter.

1.5. Literature Review

1.2.1. Rigid Polyurethane Foams

RPUFs are the most demanded insulation materials for use in construction and appliance industries due to their exceptional properties. Together with FPUFs they account for almost 50% of the polymeric foam market [8]. Besides their ease of processability, RPUFs are suitable for use in a broad range of temperatures, they possess high mechanical strength, very good chemical durability, adequate adhesive property and most importantly, they show excellent thermal insulation capability. In fact, it can perform very well even at much less thicknesses than other insulation materials like expanded polystyrene and mineral wool [3].

Polyurethane is formed through the reaction of a polyol and an isocyanate. These compounds react to form urethane bonds. RPUFs are produced from the reaction of these compounds in the presence of a blowing agent, a catalyst and a surfactant. Other liquid/solid additives may be included, such as FRs and nanoparticles, depending on the desired product. Polyol provides flexibility to the product, as the name implies, for RPUFs usually polyols of short chains are preferred. Polyester polyols possess higher thermal stability than polyether polyols. Isocyanate part provides rigidity. Aromatic isocyanates such as toluene diisocyanate (TDI) and polymeric methylene diphenyl diisocyanate (PMDI) are preferred since they are highly reactive, thermally stable and cost less. [3]. Blowing agents basically develop the foam. These agents either chemically react with polyol and/or isocyanate to produce a gas or they are liquid at room temperature and vaporize by the heat produced during foaming reaction. Blowing agents used for this purpose vary from chlorofluorocarbons, hydrocarbons, cyclo/isopentane, butanes to water (converting to CO_2 through reaction), nitrogen and air.

From an environmental point of view, blowing agents need to possess low global warming potential, zero ozone depletion potential and toxicity. Apart from these, for good insulation effect they need to be chemically inert, have low thermal conductivity, low boiling point and low diffusion coefficient in the foam. Catalysts balance the reactions during foaming while surfactants reduce surface tension and stabilize polymerizing interface [9, 10].

1.2.2. Halloysite Nanotubes

Omalius d'Halloy discovered halloysite mineral in Angleur, Belgium and it was named after him in 1826 [11, 12]. HNTs are one of the most promising natural, green nanoparticles due to countless properties they possess and research on HNTs and their applications has been extensively going on since 1940s [13]. They are abundantly available in deposits and are also thought as alternatives to carbon nanotubes (CNTs). They exhibit high biocompatibility, up to 0.2 mg/mL concentration they are shown to be safe [14], and low cytoxicity together with the low cost, which are some of the drawbacks of CNTs [15].

HNT is a 1:1 aluminosilicate clay mineral. Even though the exact mechanism is not well-known, it is accepted that rolled kaolin clay sheets form tubular Halloysite. HNTs can be found in many different morphologies, at least 10 are reported, while the most common morphologies are tubular, spheroidal and platy halloysite in decreasing order [14, 16].

HNTs possess a long, thin, tubular structure with an empty lumen - inner diameter varies from 10-150 nm and length varies from 0.2-15 microns, which corresponds to a high aspect ratio [17, 18]. Lumen width is between 10-20 nm [19]. They also have high porosity and large surface area that make them ideal for many applications.

HNTs are chemically similar to but structurally different than kaolin [20]. It is given by the chemical formula $Al_2Si_2O_5(OH)_4.nH_2O$ where n can be 0 or 2. When n=2, Halloysite is said to be hydrated and it contains a layer of water in the interlayer space. This corresponds to halloysite-10Å, but the interlayer water can be lost quite easily even in dry air, by mild heating or vacuum application. This process is irreversible and halloysite-7Å is obtained (n=0) [16]. Generally, 10-15 aluminosilicate layers form the cylinder. The outer surface of the tube is composed of tetrahedral siloxane bonds (Si-O-Si) and the inside surface is composed of octahedral aluminol bonds (Al-OH) [14]. Depending on the geographical

conditions, a small amount of the Al or Si atoms may be substituted by Fe, Cr or Ti atoms as well. Reactive hydroxyl groups are present at defect sites on the surface and at the edges of the tube [6].
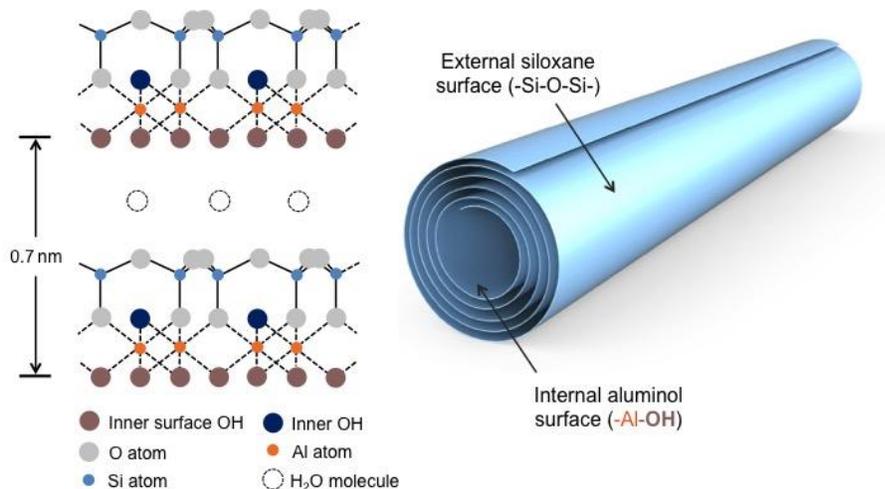
Figure 2. Halloysite nanotube [21]

HNT's outer surface has a negative zeta potential of approximately -30 mV and inner surface has a positive zeta potential of +25 mV in an aqueous dispersion at normal pH [14]. Its colloidal stability is low, it stays suspended only 1-2 hours in an aqueous solution of 6.5 pH. Dispersion stability can be improved by the adsorption of anionic species into the lumen, it was shown to stabilize the dispersion up to weeks [19, 22].

The empty lumen and the difference in the outside/inside chemistry paves the way for tuning the HNT's properties according to desired performance. Selective modification of outside/inside surfaces are frequently seen in the literature. Acid etching is used to increase the porosity and lumen space of HNT and it usually aims the Al surface. Similarly, alkali treatment is used for modifying siloxane surfaces [15, 23]. Covalent or non-covalent functionalization of surfaces with chemical species are also common. These are done in order to increase the hydrophobicity of HNTs and enhance the particle dispersion/compatibility in/with different matrices/agents. HNT is very much hydrophilic with a water contact angle of $10 \pm 3°$. For many applications it is necessary to modify its surface in order to make it hydrophobic. This becomes especially important when loading the lumen with species [24].

Clay nanoparticles tend to agglomerate due to hydroxyl groups on their surfaces. Unlike other

clay particles (such as platy ones), HNTs do not require long exfoliation processes, it is easier to disperse them [14]. They possess lower number of OH groups than many other clays, yet they still agglomerate due to their high surface energies, which results in poor dispersion. Functionalization usually helps overcome this problem but also, low hydroxyl group content on the HNT surfaces limits the reactive sites for bonding to occur [25]. It was reported that it was to possible to generate new defect sites (i.e. Si-OH) on tube surfaces by vacuum UV treatment [26].

The empty lumen of HNTs allows for the entrapment and sustained release of many biological and chemical agents for a variety of different applications. These include loading of FRs [27], drugs, antibacterials, antioxidants and other biological molecules [28-34], anti-corrosion agents [35], self-healing agents [17, 36, 37] and adsorption of dyes and pigments [38].

HNTs are mostly used as fillers for polymers for a variety of applications. They can act as mechanical reinforcers. They can be used for tailoring the crystallization behavior of polymers as well. Additionally, they are used for flame retardancy studies where they have been shown to involve in the char formation [13, 24]. They are also used in gas scavenging applications such as food packaging [39, 40], for growth of nanoparticles and catalyst supports [41, 42], water treatment and purification [43-45], tissue engineering [46, 47], cosmetics [48-50], porcelain, bone china and fine china products [51] and forensic science [52].

1.2.2.1. Functionalization of HNTs

It has been emphasized in the literature that the dispersion and distribution of nanoparticles in polymer matrix and filler-polymer interactions have great importance in polymer nanocomposites. A good dispersion of nanoparticles can greatly improve physical, mechanical, thermal properties and flame retardancy of the nanocomposite, while poor dispersion may worsen the properties even than those of the neat polymer [53, 54].

As stated before, HNT's outer surface has negative zeta potential and it is hydrophilic, for this reason it has a fairly good dispersion in aqueous solutions [24]. Also, since they are more hydrophobic compared to other clays, they are much easier to disperse in non-polar polymers.

However, this is not the case in more polar polymer matrices. Generally speaking, shear stresses (mechanical stirrers, high shear mixers) and ultrasonication are commonly used and shown to be effective in breaking the agglomerated clay structures. Even more severe shear stresses are also preferred, such as ball mill homogenization and melt extrusion [55]. The nanocomposites can be prepared by melt compounding, in situ polymerization, solution blending and others [56]. For the clay to reinforce the material, the clay gallery should be opened, meaning that the polymer should be intercalating and/or exfoliating the clay. The increased basal spacing will provide better dispersion. Otherwise, phase separation will occur and aggregation will be observed [57].

There are also some studies concerned with size separation of HNTs. Rong et al. [58] have obtained homogeneous and length-controllable HNTs by using ultrasonic scission and two-step uniform viscosity centrifugation. The effect of sonication and centrifugation time, ultrasonic power and concentration on the yield and size distribution have been extensively studied.

Chemical modifications to HNT surfaces are frequently reported for this purpose. Besides acid/alkaline etching treatments to surfaces, inner/interlayer/outer surfaces can be selectively modified and/or functionalized with chemical species to improve stability and dispersion of HNTs. These processes will surely influence the physical and chemical properties of the HNT surfaces as well. Through functionalization it is aimed to enhance both dispersion and the adhesion between matrix and filler which, in return, have a positive effect on the properties of the resulting nanocomposite product [6, 24, 59].

The functionalization of nanoparticles can be done by both physical and chemical bonding. Hydrogen bonding, electrostatic attraction and covalent bonding can be counted among these. Functionalization occurs through the exposed hydroxyl groups at the edges and defect sites on the inner Al surface, outer Si surface and interlayer Al surface of HNTs [24].

Outer surface of HNTs can be modified by alkali treatment. This can help increasing the hydroxyl groups on surface and thinning of the walls which become beneficial for functionalization and loading of the species in the lumen [59]. In most cases sodium hydroxide (NaOH) is used for this treatment [60]. For inner surface, acid treatment helps

widen the diameter of the tube since it causes dissolution of the alumina groups [15]. Hydrogen peroxide (H_2O_2) [61] and Piranha solution [53] can be other examples used for this purpose. The modification to the inner surface can be desirable for immobilization and controlled release of loaded species [62]. These modifications are usually followed by TEM imaging, nitrogen adsorption-desorption measurements and elemental analyses. On the other hand, for these treatments to be useful, HNTs should be treated in mild acid/alkaline solutions. Joo et al. [63] have shown that the pH of a solution affects the overall charge of the nanotube. In highly acidic solutions agglomeration of particles occurred. While at basic conditions, specifically at pH=11, particles were well dispersed and separated from each other. Very high concentrations of strong acid/alkaline compounds and/or extended treatment times have been observed to be detrimental to the structure of the clay [15, 23, 64].

Surface modification with organosilanes [65, 66], phosphonic/phosphoric acids [67, 68], surfactants, cationic/anionic species, polyelectrolytes [22, 59, 69] and biological species [70, 71] exist in the literature. Surfactants are used for decreasing the surface tension. Outer surface is usually modified with cationic species like polyethyleneimine and chitosan. These surfactant-modified HNTs are suitable for the formation of micelles and used for applications such as water remediation. Inner surface modification with anionic species also helps increase the HNT's stability in water, since it increases its negativity [59]. Importantly, silanes are the most common modification agents in polymer-filler nanocomposites. Functionalization of inorganic and in most cases clay surfaces via grafting of silane coupling agents is commonly reported in the literature. When functionalized particles were added into polymers, they were observed to provide good dispersion, resulting in better mechanical, thermal, moisture resistance properties of the product [53]. Phosphorus derivatives are much less sensitive to nucleophilic substitution than silicon derivatives are, because phosphorus has a higher electrophilicity compared to silicon. For this reason, in some cases phosphorus derivatives are preferred over silanes [6].

These modification agents can react with both the inner and outer surfaces, exposed Al-OH and Si-OH sites respectively. Generally, the interlayer inner surface Al-OH groups are unavailable for grafting, since they are blocked by hydrogen bonds between the layers [24]. However, it is reported in the literature that some organic molecules, such as dimethyl

sulphoxide (DMSO), can intercalate into these layers. Then, species that are normally unable to penetrate, such as γ-aminopropyltriethoxysilane (APTES), can replace these molecules and react with the surface. It is also said that the hydration state of HNT may have a positive effect on intercalation. For example, formamide is only partially able to intercalate between the layers in dehydrated state. However, depending on hydration, the intercalation degree may change [16].

The reaction of organosilanes with inorganic species that have hydroxyl groups on their surfaces involve hydrolysis and condensation reactions, which is shown in Figure 3. There are several studies describing this mechanism [6, 72]. Yuan et al. [62] have studied the grafting of HNT with APTES. Effect of evacuation and thermal treatments and degree of moisture on grafting have been extensively studied and proposed reaction mechanisms were presented. It is concluded that modification occurs through two mechanisms: grafting and oligomerization (Figure 4). Direct grafting occurs between the hydrolyzed APTES and hydroxyl groups of HNT. In the presence of sufficient physically adsorbed water on HNT, oligomerization can take place. Water causes APTES to completely hydrolyze, in this case hydrolyzed APTES molecules condense onto each other and form a crosslinked structure. Some APTES molecules can form hydrogen bonds with this structure as well. This study has shown that thermal pretreatment has a significant effect on oligomerization, samples treated at 400°C showed less oligomerization and more direct grafting. Loading of APTES into the lumen via evacuation also helped oligomerization. This will simply allow the introduction of more APTES to the inner surface.
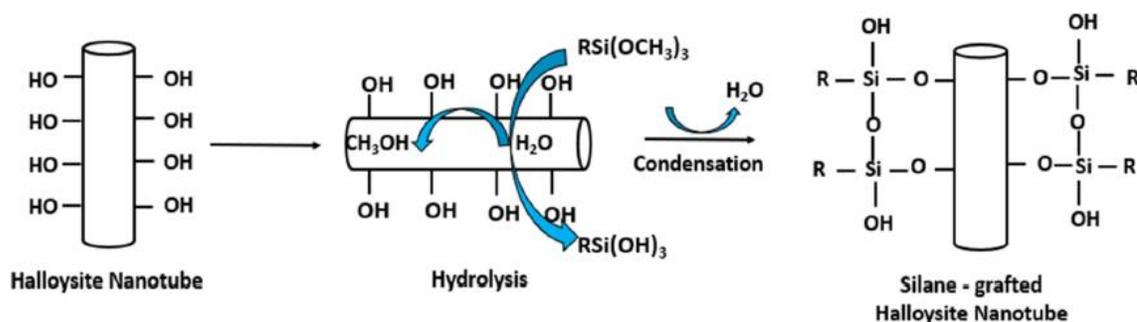
Figure 3. Grafting of silane coupling agents on HNT surface [59]
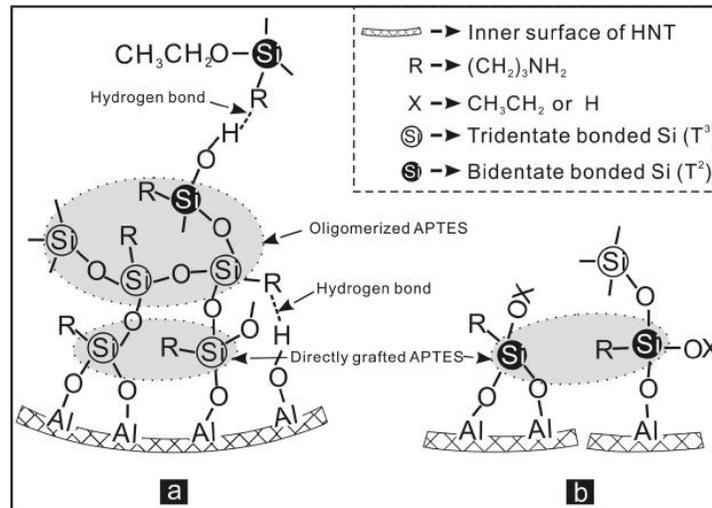
Figure 4. Formation of the crosslinked silane network [62]

Yaghoubi et al. [73] functionalized multi-walled CNTs with APTES and dipodal silane (DSi) separately and added them into RPUF matrix up to 3 wt%. It was shown that the functionalization occurred through FT-IR and TGA. Modified multi-walled CNT addition up to 1.5 wt% increased the cell density, thermal stability and mechanical properties of the foam samples which was attributed to the interactions between silanes and urethane groups and good dispersion. However, they observed poor dispersion at 3 wt% loading.

Rapacz-Kmita et al. [74] modified HNTs with APTES for a drug loading/release application. Zeta potential was shown to shift from negative to positive values after silanization and loading of the drug. TEM measurements showed that the modified HNT's lumen was filled and roughness on the surface was observable. Drug release occurred in a larger time period compared to neat HNTs.

Massaro et al. [41] functionalized HNTs firstly with 3-mercaptopropyl trimethoxysilane and further modified them with an ionic liquid. These reactions were tried by a classical procedure, microwave irradiation and solvent-free microwave irradiation and compared. The highest thiol loading of 2.2 wt% was obtained in an hour, at 80°C with microwave irradiation. With MW, but without solvent and at 100°C a loading of 2.1 wt% was obtained. However, traditional method gave 0.8 wt%, even though it lasted 20 hours at 120°C. Solvent-free methods were shown to produce higher yield.

11

Bischoff et al. [75] investigated the effect of silane type and silanization reaction conditions on the final polymer nanocomposite. Silane compounds used were triethoxy(octyl)silane (C_8) and trimethoxy(octadecyl)silane (C_{18}). Different HNT to silane ratios were tried, 5:1 and 2.5:1. Two methods, Carli method in which the reaction occurs under constant stirring in ethanol and Yuan method in which the system is refluxing in toluene were applied. Nanocomposites were melt processed. The group observed higher grafting yield when toluene was used, which was attributed to decreased silane hydrolysis that impairs oligomerization. Mechanical and thermal properties of the nanocomposites, as well as the dispersion of modified nanoparticles were seen to enhance.

Terzopoulou et al. [76] used APTES-functionalized HNTs in in-situ polymerization of ε-caprolactone monomer, because it involves in the ring opening reaction. Nanocomposites of PCL with HNTs and APTES-functionalized HNTs were synthesized with the in-situ ring-opening polymerization method. Dispersion quality was confirmed by scanning electron microscopy (SEM) characterization. Crystallization rate of the matrix was improved with fillers, which was attributed to the enhanced interfacial interactions and dispersion due to the functionalization of nanotubes. Nanotubes also helped for better nucleation of PCL matrix. Thermal stability of nanocomposites did not show a significant change with neat HNT, however it was found that APTES-modified HNTs catalyze the degradation of the polymer.

Peixoto et al. [77] functionalized HNT surface with six types of organosilanes, all possessing different functional groups, for utilization as catalyst supports for intrinsic catalysts. Morphology, structure and chemistry of the functionalized HNTs were extensively studied. Functionalization with HNT surface occurred through the alkoxy moieties, in a 3-fold or 2-fold covalent grafting or in both ways. Organosilanes containing NH_2 groups also showed NH_2-silicon oligomerization.

As mentioned, the hydroxyl groups required for functionalization are low in number on HNT surfaces. This situation usually decreases the yield of functionalization. There are a few studies addressing this problem. Jing et al. [26] used vacuum UV treatment to increase functionality of the tubes. Yuan et al. [78] have also observed increased functionality after calcination of HNT between 600°C and 900°C. They were able to partially and even completely replace siloxane groups on the outer surface with hydroxyl groups. As stated

previously, alkali/acid treatments can help as well. Another problem mentioned in the literature is related to the interlayer water. As stated above, interlayer water is desirable for intercalation of organic compounds. On the other hand, the interlayer water can have great effect on the grafting of organosilanes on HNT, since it affects their hydrolysis [24].

Chapter 2

2. Experimental Methodology

2.1. Materials

Halloysite nanotubes (HNT) in the form of 5-micron agglomerates were kindly donated by Eczacıbaşı ESAN. Isocyanate and polyol components of the two-component polyurethane foam systems and tris(1-chloro-2-propyl) phosphate (TCPP) were kindly donated by Pluskim. Three different foam systems were used throughout the study. Decoration (DEC) foam is a high density, water-blown foam, prepared at 100/105 (polyol/isocyanate) ratio. Spray (SP) foam is a rigid foam, possesses lower density, utilizes cyclopentane as the blowing agent and was prepared at 100/110 (polyol/isocyanate) ratio. B3 foam system is low density foam without any FR. B2 foam is composed of B3 formulation with 15% FR agent, TCPP. Both B3 and B2 foams were prepared at 100/105 ratio. All systems are based on polymeric diphenylmethane diisocyanate (PMDI).

3-isocyanatopropyl triethoxysilane (A-Link 25, IPTES) was purchased from Momentive Performance Materials. Polypropylene oxide-based polyol (PPO, Acclaim 2200) was provided by Bayer MaterialScience. Toluene (99.8%) was purchased from Sigma-Aldrich. Chloroform (99.8%) was purchased from Isolab. All materials were used as received.

2.2. Sample Preparation and Synthesis

2.2.1. Processing, Loading and Functionalization of HNT

2.2.1.1. Processing of HNTs:

Untreated or sonicated HNTs were incorporated into foam compositions. For sonication, 1 gram of HNT was dispersed in 100 mL of distilled water at an amplitude of 35 for half an hour. Water was removed via Rotary evaporator and obtained HNT powder was dried in oven at 110°C. Dried powder was later grinded in a mortar and became ready to use. Samples labeled with an "S" indicates, sonicated HNTs, samples labeled with "U" indicates unprocessed HNTs.

2.2.1.2. Loading of HNTs:

For the loading of the FR agent into the nanotubes, 0.5 g of HNT was added to a round-bottom flask and excess TCPP was added on top covering HNTs. The flask was stirred and placed under vacuum for 10 minutes. Bubbles formed on the surface due to the air coming out of the nanotubes was observed. When the vacuum was broken, FR agent diffused into the tubes. This process was repeated 3 times to provide higher loading. Product was washed twice with ethanol and collected by centrifugation and let dry at room temperature. Loaded HNT (denoted as L-HNT) was pounded in a mortar and then added to B3 foam formulations. Scheme 1 shows the process schematically.
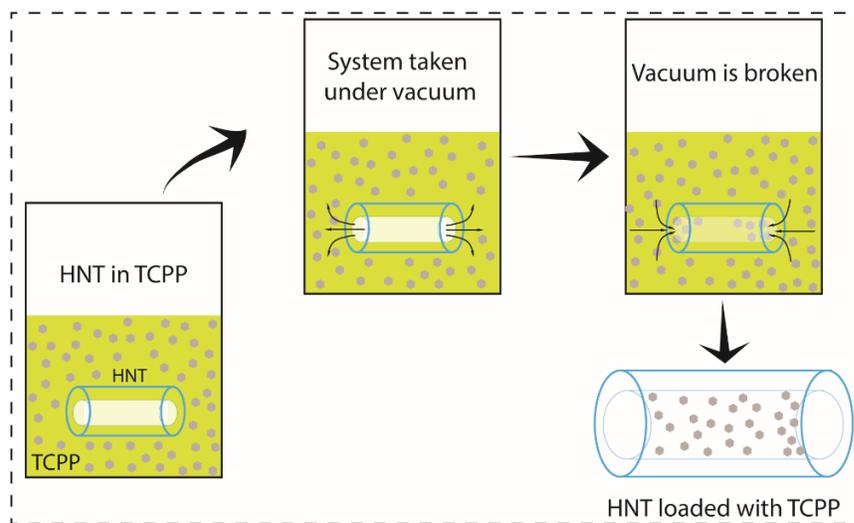
Scheme 1. FR loading of HNTs via vacuum cyclization

2.2.1.3. Surface Functionalization of HNTs:

PPO was added into a flask, heated to 100°C and dewatered via vacuum. Then, IPTES was added to provide 1:1 molar ratio. Under nitrogen atmosphere, the system was mixed at 80°C

and the reaction was followed with Fourier transform infrared spectroscopy (FT-IR) by ensuring the disappearance of the isocyanate peak around 2270 cm^{-1}. HNT, dried at 110°C overnight and sonicated for 30 minutes (amplitude: 40, on/off: 5/3 secs) in dry toluene, was added into the mixture. Reaction refluxed for 4 days at 80°C. Product was obtained via centrifuge, washed two times with dry toluene and three times with chloroform and later dried in vacuum oven at 70°C. The synthetic route is given in Scheme 2.
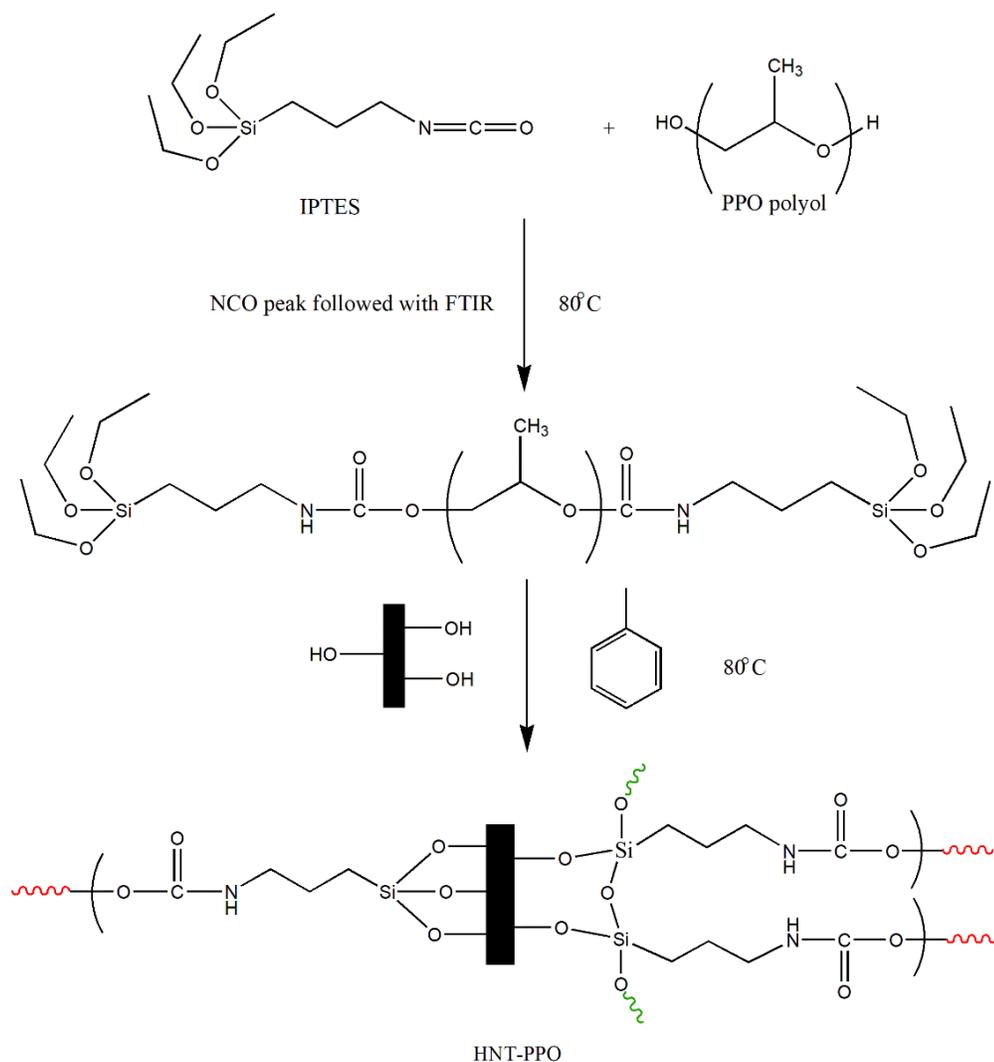
Scheme 2. Surface functionalization of HNTs with PPO using IPTES as coupling agent

2.2.2. Foam Preparation

HNT was added into foam formulations at different weight ratios with respect to the polyol component. The polyol component and HNT were mixed with a planetary mixer for three

16

minutes. Required amount for both polyol and isocyanate components were weighed into plastic cups, the mixture was mixed with a mechanical stirrer at 2000 rpm for 7-10 seconds and then let to rise in the cups or poured into a mold for the foam formation.

For foam samples containing HNT-PPOs, after mixing the polyol and HNT-PPOs with a planetary mixer, the mixture was further subjected to ultrasonication for 20 minutes (amplitude: 50, on/off: 5/30 secs) prior to mixing with the isocyanate component and foam formation followed the same procedure above.
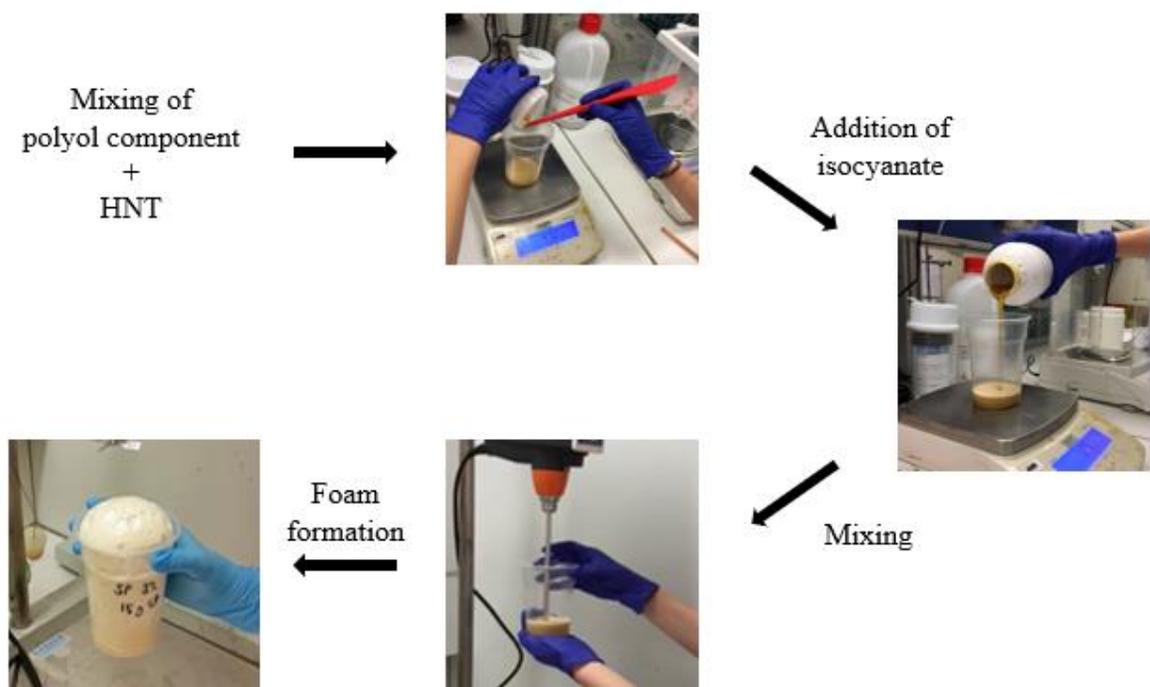
Figure 5. Preparation of foams

2.3. Characterization

Functionalization reaction and modified HNTs were characterized with Nicolet IS10 Fourier Transform Infrared Spectrometer (FT-IR) with an ATR system, at a resolution of 4 with 128 scans.

Densities of the foams were determined following ASTM D1622 standard. Mass to volume ratios of samples were measured.

Scanning electron microscopy (SEM) measurements were conducted on Zeiss LEO Supra 35VP SEMFEG instrument. Cryogenically broken surfaces were coated with Au-Pd. Unless stated otherwise, all SEM images were taken at 200X magnification and 3 or 5 kV accelerating voltage. Cell sizes and aspect ratios were measured from these images using ImageJ software.

Thermogravimetric analysis (TGA) were done on Shimadzu DTG-60H. HNT samples were heated from 30°C to 1000°C with a heating rate of 10 K/min, under 100 mL/min nitrogen flow.

Thermal conductivity measurements were done with Hot Disk Thermal Constants Analyzer, TPS 2500S. All measurements were conducted with Kapton disk with radius 6.403 mm at room temperature. Measurement time and output power were between 80-160s and 3-10 mW respectively and determined according to the sample type. The machine operates according to the transient plane source (TPS) method, which is regarded as the most convenient and accurate technique for measuring thermal transport properties. A transiently heated sensor is placed between two identical pieces of the sample. The sensor consists of an electrically conductive metal pattern which is covered between two thin sheets of an insulating material. During the measurement, an electrical current is run through the sensor, which increases the temperature of the sensor and the sensor measures the resistance of the sample at the same time. Testing setup is seen in Figure 6.

Figure 6. Thermal conductivity measurement setup

Viscosities of foam components were determined with Brookfield viscometer. Spindle #27 (B3, 150 rpm and B2, 200 rpm) and spindle #21 (PMDI, 100 rpm) were used.

2.3.1. Flammability Tests

Small flame test was done according to the TS EN ISO 11925-2 standard. In this test, a flame like that of a lighter flame, is applied to the material surface with a degree of 45 for 15 seconds. At the end of this period, it is observed whether the flame can reach from the point of flame application to a 150 mm limit in a certain time. Formation of flaming drips were also evaluated with this test. For this test, SP, B3 and B2 foam samples that contain 0, 1, 5 and 10% HNT were prepared by pouring in 250x90x50 mm molds, specified by the test. Molds and preparation process are shown in Figure 7.

Figure 7. Sample preparation for small flame test

An in-house flame test setup was also designed to gain an insight about DEC and SP foams' flammability behaviors. Tests were conducted at about 30°C under atmospheric conditions. At least two test specimens of each samples with dimensions of about 150x30x15 mm were prepared in molds. The samples were clamped at a degree of about 45 to the horizontal and were subjected from a distance of 30 mm to a 70% butane/30% propane mix flame of 50 mm length for 30 seconds. Average time it takes for the samples to extinguish themselves was measured. The test setup and actual testing photos are shown in Figure 8 and Figure 9, respectively.
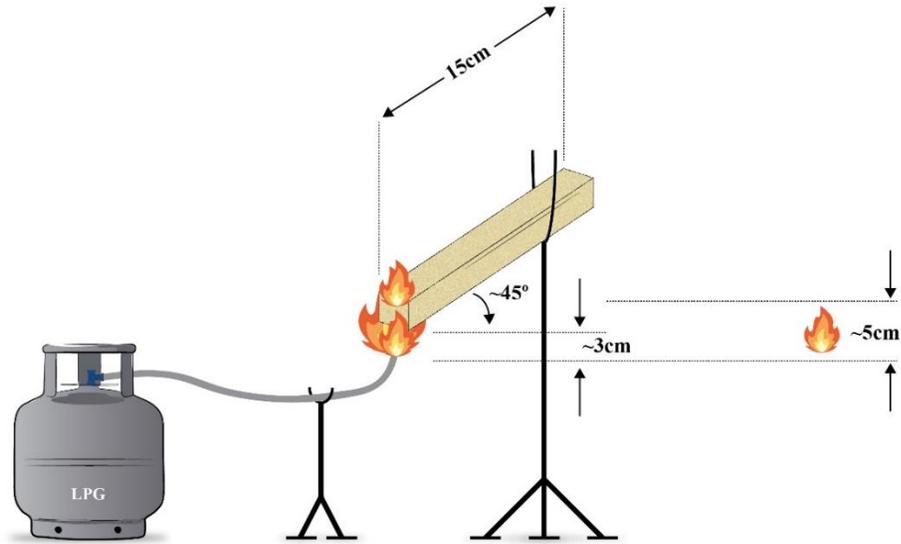
Figure 8. Diagram showing the setup prepared by us

Figure 9. Samples and testing for our setup

In order to determine the minimum concentration of oxygen that is needed for the material to sustain burning, limiting oxygen index (LOI) for samples was determined with Deatak Oxygen Index Test Apparatus, OI-3 model, according to ASTM D2863. 15 specimens for each sample with dimensions 130x10x10mm were prepared and tested. In the LOI test, a candle-like sample is put into the cylindrical chamber and ignited. Constant flow of oxygen is provided at pre-determined percentages and the sample is observed whether it burna completely or self-extinguishes.

Cone calorimeter (CC) measurements were done with Deatak Cone Calorimeter CC-2, according to ISO 5660. Samples were irradiated in a horizontal position at 50 kW/m^2. Three

test specimens with dimensions 100x100x25mm were prepared for each sample. CC operates on the oxygen consumption principle, in which, amount of oxygen used in the combustion process is directly proportional to the released heat [79]. It also gives quantitative data on smoke production, CO and CO_2 yields, and residual mass. Figure 10 shows sample testing with cone calorimeter.
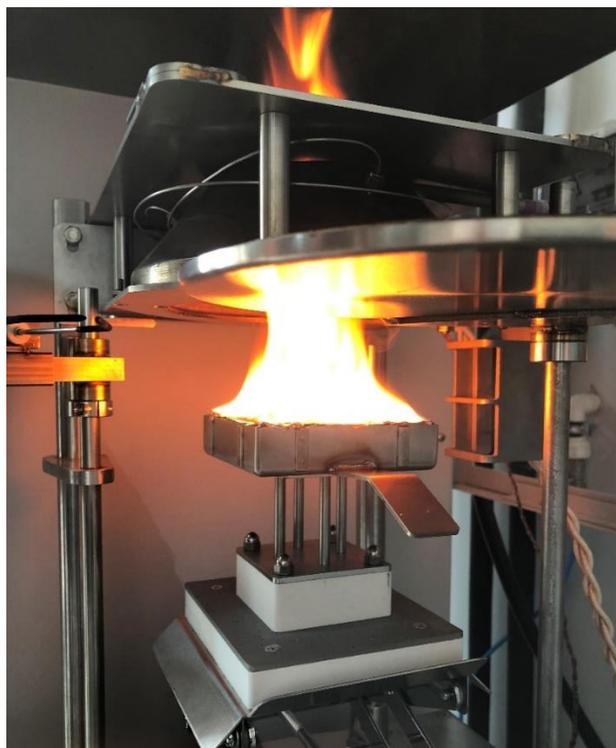
Figure 10. A foam sample being tested with a cone calorimeter

Specific optical densities of samples were measured with Deatak SD-2 model smoke density chamber, following ISO 5659-2. Three test specimens with dimensions 75x75x25mm were prepared and tested for each sample at only one mode, with a pilot flame and 25 kW/m^2 irradiation.

Average values were reported for each test.

Chapter 3

3. Morphology and Thermal Conductivity of RPUFs

3.1. Introduction

3.1.1. Thermal Conductivity of RPUFs

Thermal conductivity performance of RPUFs depend especially on the following: cell size, the type of gas trapped inside the cells (i.e. blowing agent), foam density, open/closed cell ratio and cell orientation. It is also less dependent on the following: isocyanate index, type of chemicals [80]. Modification in PU's versatile chemistry and using additives that will absorb, reflect or scatter radiative energy are two ways to decrease thermal conductivity [3]. It is commonly reported in the literature that liquid/solid additives such as nucleating agents and various nanoparticles are capable of influencing thermal conductivity [81-83]. As they are enhancing insulation capability, they also mechanically reinforce the matrix without necessarily worsening other properties. They have a strong influence on the structure, rheological properties and density of the material as well [84].

As the cell size gets smaller, thermal conductivity tends to decrease. Additives can influence the formation of the foam, acting as nucleation points, they contribute to the formation of smaller cells and a more uniform cell distribution [80, 85]. Liquid additives incorporated into the foam formulations may contribute to the cell size reduction better than solid additives at higher amounts. Solid additives at high amounts may increase the matrix viscosity greatly to create a high surface tension and as a result, nucleation requires higher energy [86]. Viscosity increase has a strong effect on cell formation. It has been reported that the large surface area and small dimensions of nanoparticles provide better contact with the matrix, particles and gas. Solid particles added to a liquid matrix cause a decrease in Gibbs free energy, facilitating

22

heterogeneous nucleation. The energy barrier for heterogeneous nucleation is lower than that of homogeneous nucleation, due to close contact between the matrix, gas and particles [84]. Lorusso et al. [84] hypothesized that HNT becomes a bigger obstacle in the mixing of the PU foam mixture than TiO_2 in their study, arising from its rod-like shape. Compared to spherical TiO_2, it has stronger effect in lowering the Gibbs free energy, creating more nucleation and decreasing cell size more effectively.

There is a wide range of nanoparticles used for changing the thermal conductivity of foams, both to increase and decrease. Ultrasonication and simple mixing are used commonly to incorporate these particles.

Thirumal et al. [80] incorporated an organically-modified clay to RPUF matrix. Up to 5 php (parts per hundred polyol by weight) clay addition, cell size was observed to decrease. Above that, cells were ruptured, arising from excessive coalescence. Thermal conductivity followed the same trend as well, it decreased with decreasing cell size, while increasing at a loading of 10 php.

Kang et al. [87] tried one liquid silane-based and two solid nucleating agents, a clay and a SiO_2 powder. They concluded that liquid additive was better at decreasing the cell size, by lowering surface tension. Solid additives in large amounts strongly increase viscosity, so energy needed for nucleation increases. With addition of agents up to 3 phr (parts per hundred resin), consistent decrease in cell size and thermal conductivity was observed. Additionally, solid particles caused the rupture of cell walls, reducing the closed cell content. This paves the way for increased gas diffusion, in and out of the foam, causing an increase in thermal conductivity eventually. Liquid additive did not affect the closed cell content significantly. It was also emphasized that fillers with micron-scale dimensions aggregate easily and their influence on foam expansion is greater which will form a worse structure.

Estravís et al. [88] filled RPUFs with different amounts of organo-modified montmorillonite (MMT) clays and studied their time-dependent thermal conductivity. Water-blown foams showed rapid diffusion of CO_2 in the first ten days, to be replaced by the atmospheric air and therefore increasing the thermal conductivity. Diffusion slowed down up to 40 days, then reaching a stable state.

Lorusso et al. [84] used HNT and spherical TiO_2 as reinforcers, separately. The group observed an increase in cell density with increasing filler concentration. Foams added with HNTs showed a decrease in thermal conductivity up to 8 wt% concentration and mechanical properties were also enhanced. Thermal conductivity value was 0.026 W/m.K for the neat foam after 10 days, this value stayed the same at 2, 6 and 8% HNT, but increased to 0.030 W/m.K at 10% HNT loading. Whereas, for both types of nanoparticles at a concentration of 10%, conductivity was worsened and rupture of the cell walls was observed. TiO_2 particles are claimed to be gathered at the cell walls rather than at the nodes, increasing the wall thickness and providing better mechanical behavior. It was concluded that HNT performs better than TiO_2, this was attributed to its elongated shape which decreases the nucleation energy.

Qi et al. [89] prepared crude glycerol-based RPUFs incorporated with HNTs and microcrystalline cellulose (MC). Viscosities, thermal and mechanical properties of the composites were studied. Viscosity is an important parameter, since it affects the foaming reaction. 5 wt% HNT addition resulted in increasing the viscosity by 82%, reaching 1102 mPas. However, at 5 wt% MC addition the viscosity value was 807 mPas. This difference was attributed to better dispersion of HNTs in the polyol matrix. HNT incorporation helped to decrease the cell size, which could be due to the effect of increased viscosity negatively affecting the mixing of components and the increased number of nucleation sites. At 5 wt% HNT loading, foams had bigger cells, which was attributed to excessive cell coalescence. Both density and compressive strength showed an increase with 1 wt% HNT addition, however both values decreased with further increase in HNT content. Thermal conductivity values did not change significantly. Also, the thermal stability of foam samples was not influenced by the incorporation of HNTs, which could be due to the limited effect of HNTs as heat barriers.

3.1.2. Theoretical Basis of Thermal Conductivity in RPUFs

The insulating capability of porous insulators have been of interest and there are many studies in explaining how insulation occurs in such materials. The theoretical basis of thermal conduction in PU foams has been extensively studied since 1980s. The thermal conductivity performance of PU foam is controlled by three mechanisms: solid conduction, radiation and

gas conduction [90]. Figure 11 shows a schematic of heat transfer mechanisms in closed-cell PU foams. The effective thermal conductivity of an optically thick foam [91] is given as a summation of these contributions:

$$k_{foam} = k_{solid\ conduction} + k_{radiation} + k_{gas\ conduction}$$

Equation 1. Overall thermal conductivity of polyurethane foam
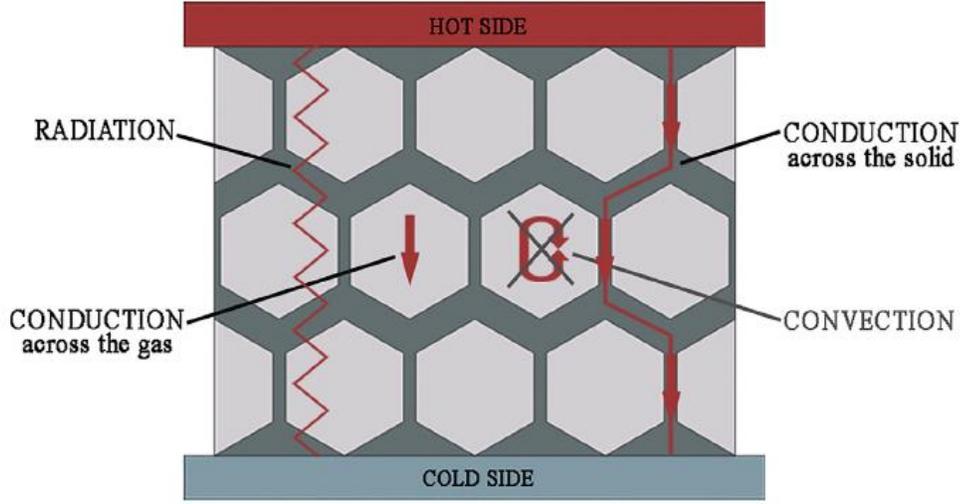
Figure 11. Heat transfer mechanisms in closed-cell polyurethane foams [92]

Solid heat transfer describes the conduction through solid polymer matrix. Its contribution to overall thermal conduction varies from 20-30%, as given in the literature [90]. The solid conduction can be varied by density, distribution of mass between cell windows and struts and chemical structure of the foam [3]. Except for the density, these parameters are not easily controllable. In general, it can be said that as the density increases, solid conduction increases as well but the overall performance will also depend on what happens with radiative conduction. Equation 2 below describes the solid conduction in foam:

$$k_{solid\ conduction} = k_{polymer} * \frac{(1-\delta)}{3} * \left[f_{strut} * \left(\frac{a}{b}\right)^{0.5} + 2 * (1 - f_{strut}) * \left(\frac{a}{b}\right)^{0.25} \right]$$

Equation 2. Solid conduction [90]

where, $k_{polymer}$ is the solid, bulk polymer thermal conductivity, δ is porosity (void fraction), f_{strut} is the fraction of solid in the struts and a/b is the aspect ratio of cells. Cell diameter

perpendicular to the temperature gradient is a and parallel to the temperature gradient is b. Porosity can be calculated from $\delta = 1 - (\rho_{foam}/\rho_{polymer})$, where ρ_{foam} is foam density and $\rho_{polymer}$ is bulk polymer density [93]. Ahern et al. [94] noted $\rho_{polymer}$ to be 1200 ± 50 kg/m^3, which covers the range of values reported in literature. Solid fraction in struts can be taken as a constant, Reitz et al. [95] has found that cell struts contain 80-90% of the solid. Nielsen et al. [96] found $k_{polymer}$ to be between 0.19-0.21 W/m.K, while Ahern et al. [94] found 0.21-0.24 W/m.K at 20°C, via hot wire technique on milled foam. Glicksman [90] gave a value of 0.262 W/m.K, for a crushed foam that was pressed until a constant value is reached in the measurement. Biedermann et al. [91] measured this value to be 0.205 W/m.K at 25°C for crushed foam. The group also did measurements on cold cured PU resins, with different additives, obtaining values between 0.16-0.21 W/m.K. Equation 3 was also proposed for temperature-dependent thermal conductivity of the bulk polymer:

$$k_{polymer}(T) = 197 * (1 + 0.0017 * T) \, 10^{-3} \text{ W/mK}$$

Equation 3. Temperature-dependent polymer thermal conductivity

It was also noted that the difference in chemical structure of PU and additives such as FRs did not significantly change the thermal conductivity of the bulk polymer, leading to the derivation of the equation above [91].

Radiation is responsible for about 13% overall thermal conductivity, sometimes as high as the contribution of the solid conduction, and is dependent on the structure and opaqueness of the cells [3, 90]. Radiation can travel through transparent and thin cell windows but not opaque struts. Rosseland equation is used for describing radiation in foams. This is useful when the mean free path of radiation is smaller than the foam thickness and it assumes isotropic foam structure. From this model it is suggested that one of the ways to decrease radiative heat transfer is to decrease cell size. Decreasing cell size means decreasing the mean free path of photons, so they will not be able to travel as much. In other words, when cell size is smaller, radiative rays will come across opaque struts more frequently, which will prevent radiative conduction. Schuetz et al. [97] has reported that the radiation behavior in polymeric foams is absorption dominated and struts block radiation by absorption and anisotropic

scattering. Another way suggested is to change the foam chemistry to change the cell wall extinction coefficient, yet PU foams generally have similar extinction coefficients.

$$k_{radiation} = \left[\frac{16}{3 * K_e}\right] * \sigma * T^3$$

$$K_e = \frac{4.10}{d} * \left(f_{strut} \frac{\rho_{foam}}{\rho_{polymer}}\right)^{0.5} + (1 - f_{strut}) * \left(\frac{\rho_{foam}}{\rho_{polymer}}\right) * K_{e,\ cell\ wall}$$

Equation 4. Radiation [90]

In Equation 4, K_e is the extinction coefficient, d is cell diameter, K_e, cell wall is the cell wall extinction coefficient, σ is Stefan-Boltzmann constant (0.0000000567 $W/m^2.K^4$) and T is the absolute temperature. Cell wall extinction coefficient can be measured via transmissivity measurements as reported in literature [98]. Wenzhen et al. [99] gave $K_{e,\ cellwall}$ as 600 cm^{-1}, as suggested by Sinofsky. Glicksman [90] also gave in his book 1633 cm^{-1} and 1100 cm^{-1}, from different references.

Gas conduction has the biggest contribution in the thermal insulation. Its share is given around 50-70% in the literature [100]. This contribution to thermal conductivity depends on the thermal conductivity of the blowing agent filling the foam cells. Using a low thermal conductivity blowing agent in the formulation is good enough of a start to have good insulation performance. However, gas conduction might be constantly changing due to the diffusion phenomenon. In time, the air is expected to diffuse into the foam cells and replace the blowing agent. It should be noted that the air is composed of smaller molecules compared to many common blowing agents. Increasing temperature will cause increased diffusion. Atmospheric gases typically have higher thermal conductivity than blowing agents. Several ways are suggested to delay this aging action. One is to choose blowing agents that have slower diffusion rates through the foam. Another is to alter the foam chemistry to introduce thicker cell walls into the structure, which makes it harder for diffusion. For sure, the composition and therefore the conduction of the gas will be different throughout the foam because of this phenomenon. Diffusion will be more apparent towards the surface, rather than the center [101]. The equation for gas conduction below was first derived by Wassiljewa in 1904 [102] and was further developed by Lindsay and Bromley in 1950 [103]:

27

$k_{gas\ conduction}$

$$= \sum_{i=1}^{N} \frac{y_i k_{gi}}{\sum_{j=1}^{N} \frac{y_i}{4}\left[\left\{1 + \left(\frac{\mu_i}{\mu_j}\left(\frac{M_j}{M_i}\right)^{0.75} * \frac{1 + 1.5 * C_0 * \frac{\sqrt{T_{bi}T_{bj}}}{T}}{1 + 1.5 * \frac{T_{bj}}{T}}\right)^{0.5}\right\}^2 \left\{\frac{1 + 1.5 * C_0 * \frac{\sqrt{T_{bi}T_{bj}}}{T}}{1 + 1.5 * \frac{T_{bi}}{T}}\right\}\right]}$$

Equation 5. Gas conduction

Where, N is the number gas species in mixture, y_i is the mole fraction of ith component, k_{gi} is the thermal conductivity of the pure ith component, μ is the viscosity of the pure ith component, M is the molecular weight, C_0 is a constant, T_{bi} is the absolute boiling temperature at 1 atm of pure ith component and T is the absolute temperature. C_0 is taken as 1 for nonpolar gases and 0.73 when one of the gases in the mixture is polar [90].

Convection contribution is not considered in the case of PU foams. This is because cell size in PU foams is too large, which makes it nearly impossible for free convection to start. Therefore, convection contribution is generally accepted as highly negligible [93].

The solid conduction and radiation are strongly dependent on the density of the foam. From Figure 12 it is seen that the lowest thermal conductivity value is obtained when the density is about 40-50 kg/m³. In general, radiation and solid conduction are correlated. At low densities, radiative conduction is high. A decrease in density will also decrease thermal conduction in the solid phase of the foam but will increase radiation because of thinner cell walls [104]. However, after a certain density value polymer conduction dominates and radiation loses its effect, thermal conductivity can start to increase. It is also seen that gas conduction contribution to overall thermal conductivity changes only by 10% over a range of densities. On the other hand, Glicksman has shown that gas conduction is almost constant as the density changes as depicted in Figure 13 [90]. In addition to these, temperature also has a determining effect on radiation and gas conduction contributions. Radiation tends to increase with increasing temperature, whereas gas conduction tends to decrease (Figure 14).

Porosity is also another important parameter, which is closely related to the density. Ferkl et al. [93] have studied porosity extensively. Conduction is expected to decrease with increasing porosity, because air is less conductive than the polymer. On the other hand, increased

porosity leads to increased radiation, because thermal radiation is absorbed less when the solid content is lower. Additionally, they also claim that in the studied porosity range, from 0.9 to 1, the gas phase in the foam increases by 10%. However, that would not lead to a significant change in k_{gas}.
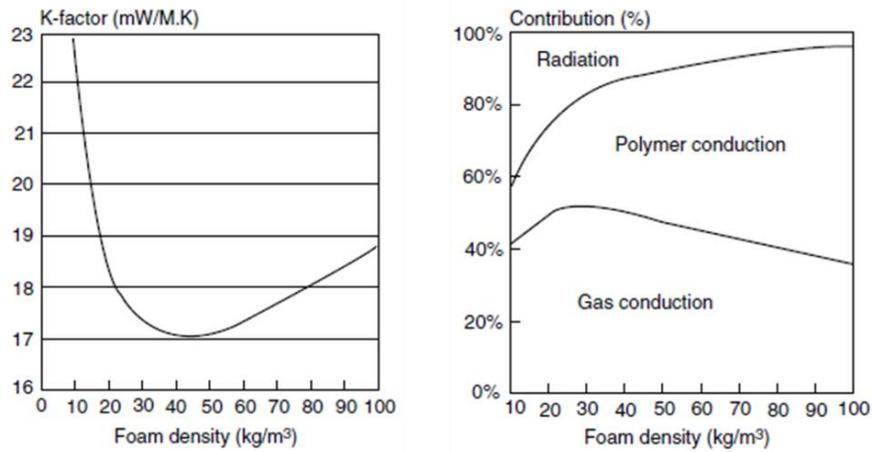
Figure 12. The change in thermal conductivity and percent contributions with density [3]
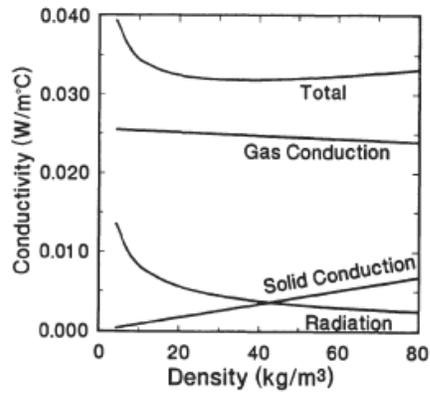
Figure 13. Theoretical change in thermal conductivity for air-filled foam over a range of densities at T=20°C [8]
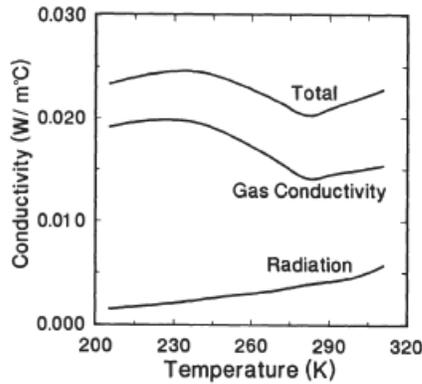
Figure 14. Thermal conductivity versus temperature for foam filled with CFC-11-air mixture at 0.6 atm [8]

To conclude, solid conduction and radiation contributions are related to the foam morphology, whereas gas conduction is independent of this. On the other hand, gas conduction changes over time, but solid conduction and radiation are not necessarily changing, since foam morphology is almost stable. If the blowing agent is decided, the thermal insulation capability can further be enhanced by decreasing solid conduction or radiation. Density is very much related to the dimensional stability of the foam, for this reason there will be limitations on it. As a result, the best option to decrease thermal conductivity is to influence the radiative heat transfer. Certainly, decreasing the cell size to introduce more opaque struts can help. Moreover, radiation is affected by the polymer's capability to absorb radiative energy. Foam chemistry may have a small, negligible, influence on this. However, additives which may absorb, reflect or scatter radiative energy can be added to the formulations, which will also have a great effect on the morphology of the foams [3, 90].

Ferkl et al. [93] used quantum chemical calculations, molecular dynamics simulations and then used homogeneous phase approach (HPA) to model thermal conductivity parameters of PU foams. The group calculated the effective gas and polymer conduction and radiative properties were determined. Morphological parameters obtained from prepared PU foam samples were used in the calculations. Theoretical and experimental data were shown to be in good agreement.

Choe et al. [105] investigated the threshold cell diameter for thermal insulation performance. They used water blown RPUFs and influenced the cell size by using different amounts of surfactants and gelling agents which change the reaction rate. The group also studied the change in radiative thermal conduction and average extinction coefficient as a function of cell size.

Coquard et al. [106] investigated the suitability of HPA and multi-phase approaches (MPA) for predicting radiative thermal conductivity of foams. Many of the theoretical studies are based on HPA. In HPA, the radiative behavior of the composite material is "matched faithfully by an equivalent homogeneous semi-transparent medium". Glicksman's method given previously also uses HPA. In MPA method, each phase has its own transport equation, which are coupled to each other, and their own radiative characteristics. They used a closed-cell polymeric foam and an open cell metallic foam to model. However, they found that HPA gives good enough approximations for polymer foams. Whereas, MPA cannot predict satisfactory spectrometric values and so is not suitable to model radiation in polymeric foams.

Wenzhen et al. [99] reconstructed models to investigate the effects of temperature, porosity and cell size on effective thermal conductivity of PU foams. The group used finite volume method and lattice Boltzmann method to give theoretical predictions of thermal conductivity and then compared these results to measured data to observe good agreement.

3.2. Results and Discussion

3.2.1. Thermal Conductivity of HNT Containing RPUFs

The initial work to investigate the effect of HNTs on the morphology and thermal conductivity of RPUFs was conducted using DEC, SP and B3-B2 foam formulations by the direct incorporation of unprocessed (as is) or ultrasonically treated (sonicated) HNTs in the polyol component.

For the theoretical calculation of the thermal conductivity of foam samples, cell diameter, aspect ratio and foam density were determined for each sample. In an attempt to also determine the conductivity and density of the solid polymer, the blowing agent was evaporated from the polyol component under vacuum and heat via a rotary evaporator for

several hours, which was then reacted with PMDI to produce bulk polymers. However, measured $k_{polymer}$ and $\rho_{polymer}$ were significantly lower than the reported values in the literature. An SEM image of one of these bulk polymers is shown in Figure 15, which clearly still have a porous morphology and confirms that the process is unsuccessful. For this reason, values from the literature were used for $k_{polymer}$ and $\rho_{polymer}$.
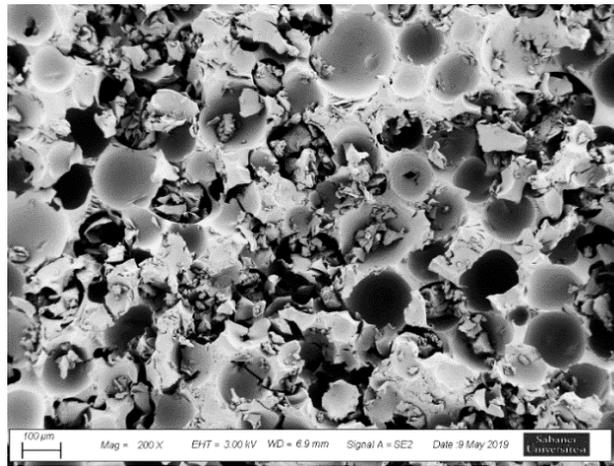
Figure 15. SEM image of foam resin after curing after unsuccessful evaporation of the blowing agent

In Figure 16 and Figure 17, SEM images for DEC foams with 1, 3, 5 and 10 wt% HNT along with the reference (0 wt% HNT) are shown for unprocessed and sonicated HNTs, respectively. Table 1 summarizes the morphological and theoretical data for each sample and Figure 18 compares the calculated and measured thermal conductivities. By comparison, it is seen that the calculated values are below the measured ones by at least 0.02 W/m.K. Most probably, $k_{polymer}$ of the DEC resin without blowing agent is higher than the assumed value. Theoretical calculations do not show the same trend as the measurements. Thermal conductivity shows a decrease up to 5% HNT loading; however, theoretical data first shows an increase then a decrease. Calculated thermal conductivity of the samples prepared with the unprocessed HNT shows a continuous decrease. As for 10% HNT loading, thermal conductivity decreased theoretically but measurements showed otherwise. The change in cell shapes, rupturing of cell walls and inhomogeneity in cell size can explain both the fluctuations in experimental data and the inconsistencies in theoretical calculations. As seen from the SEM images, cell size distribution in some samples is quite wide, especially in those

with unprocessed HNT. Also, for example in Figure 16 (e) and Figure 17 (b), cell shapes seem to become elliptical. It is seen that the samples do not have an ideal, homogeneous structure. SEM images and density measurements are used for the theoretical calculations. As a result, deviation in calculations is also possible.
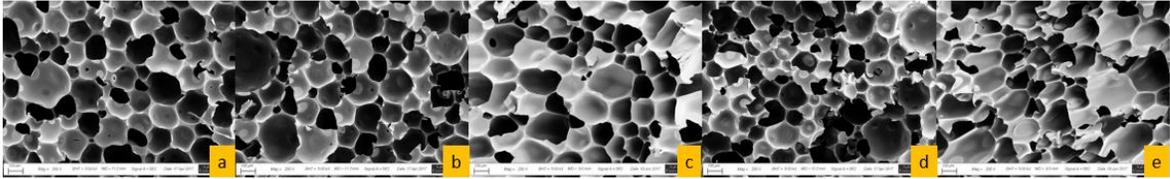
Figure 16. SEM images of DEC foams with unprocessed HNT: (a) reference, (b) 1%, (c) 3%, (d) 5%, (e) 10%
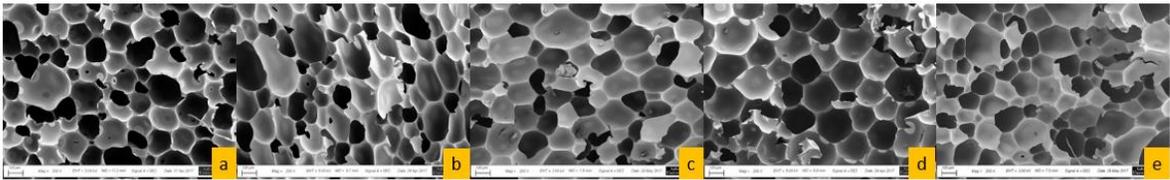
Figure 17. SEM images of DEC foams with sonicated HNT: (a) reference, (b) 1%, (c) 3%, (d) 5%, (e) 10%

Table 1. Morphological parameters and theoretical solid conduction and radiation for DEC foams

Decoration Foam						
HNT (%)	Porosity	Aspect ratio	Average cell diameter (μm)	Foam density (kg/m³)	k_solidcond (W/m.K)	k_radiation (W/m.K)
Reference	0.89	0.978	192	131	0.01132	0.00105
1-S	0.89	1.589	154	135	0.01431	0.00086
3-S	0.91	1.181	207	113	0.01057	0.00122
5-S	0.89	1.073	213	130	0.01171	0.00115
10-S	0.91	1.481	214	110	0.01130	0.00128
1-U	0.90	1.019	186	124	0.01095	0.00106
3-U	0.92	1.399	221	95	0.00955	0.00143
5-U	0.91	1.030	162	108	0.00950	0.00102
10-U	0.94	1.826	219	72	0.00813	0.00166

f_strut: 0.8, k_decpolymer: 0.22 W/m.K, K_e,cellwall: 600 cm^{-1}, σ: 0.0000000567 $W/m^2.K^4$, ρ_decpolymer: 1200 kg/m^3, T: 298.15 K (R.T.), k_gas: 0.015 W/m.K
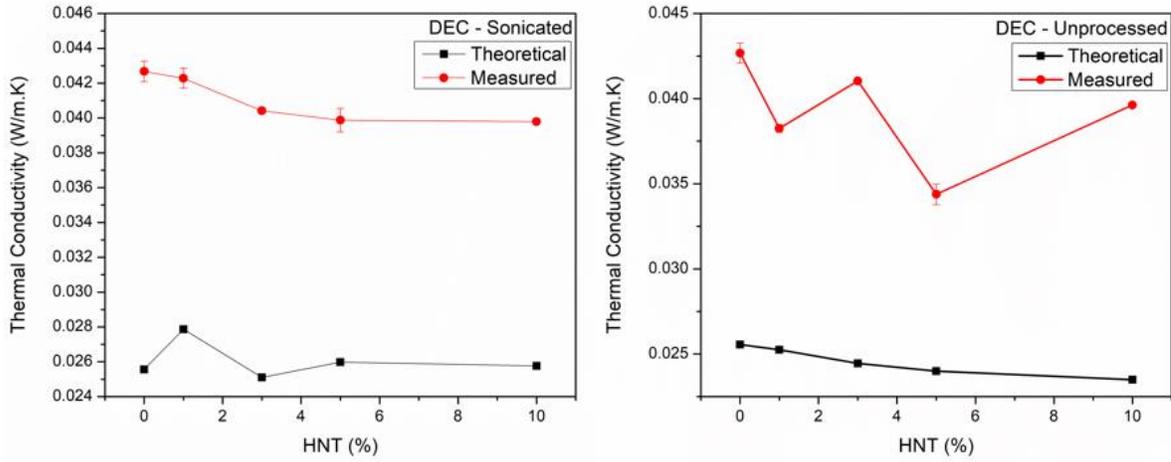
Figure 18. Theoretical and measured thermal conductivity values for DEC foams

In Figure 19 and Figure 20 SEM images for SP foams with unprocessed and sonicated HNTs are given, respectively. Table 2 summarizes morphological and theoretical data and Figure 21 compares the calculated and measured thermal conductivities. Thermal conductivity, which increased up to 3% HNT addition, showed an opposite behavior in the calculations. At 5% HNT loading, measured value is seen to be decreasing further, whereas calculated value is increasing. Reaching 10% loading, both values increased. Except for the reference and 3% HNT containing foams, the curves for measurements and calculations seem comparable. However, theoretical calculations are below the measured values, by at least 0.01 W/m.K. It should also be noted that, the measured thermal conductivity of HNT is 0.047 W/m.K, which is significantly higher than the thermal conductivity of the SP foam. Therefore, the increase in measured values should be attributed not only to the morphological changes, but also to the HNT itself.
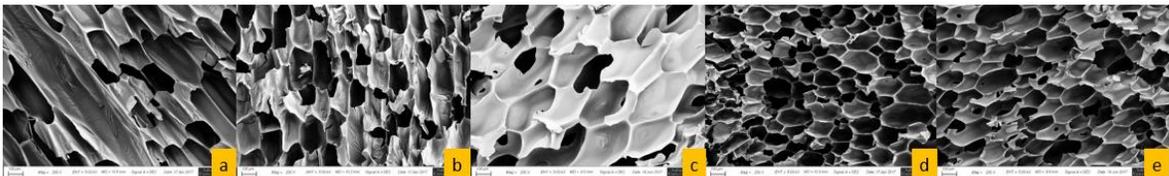
Figure 19. SEM images of SP foams with unprocessed HNT: (a) reference, (b) 1%, (c) 3%, (d) 5%, (e) 10%
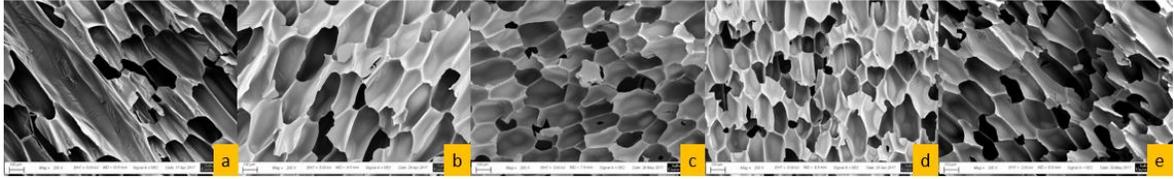
Figure 20. SEM images of SP foams with sonicated HNT: (a) reference, (b) 1%, (c) 3%, (d) 5%, (e) 10%

Furthermore, cell anisotropy is observed in almost all samples. Cells that are elongated in the heat transfer direction are known to lead to higher radiative heat transfer [90]. Confirming this, radiation contribution is seen to be higher in SP foam than it is in DEC foam.

Table 2. Morphological parameters and theoretical solid conduction and radiation for SP foams

Spray Foam						
HNT (%)	Porosity	Aspect ratio	Average cell diameter (μm)	Foam density (kg/m^3)	k_solidcond (W/m.K)	k_radiation (W/m.K)
Reference	0.95	3.587	186	34	0.00440	0.00216
1-S	0.94	2.624	176	40	0.00446	0.00190
3-S	0.94	1.992	160	42	0.00416	0.00169
5-S	0.93	2.140	142	45	0.00453	0.00147
10-S	0.94	2.843	154	43	0.00491	0.00162
1-U	0.94	2.013	148	43	0.00423	0.00157
3-U	0.95	2.125	234	37	0.00368	0.00259
5-U	0.94	1.928	173	41	0.00399	0.00185
10-U	0.93	2.059	127	49	0.00492	0.00126
f_strut: 0.8, k_sppolymer: 0.22 W/m.K, K_e,cellwall: 600 cm^{-1}, σ: 0.0000000567 W/m^2.K^4, ρ_sppolymer: 1200 kg/m^3, T: 298.15 K (R.T.), k_gas: 0.013 W/m.K						
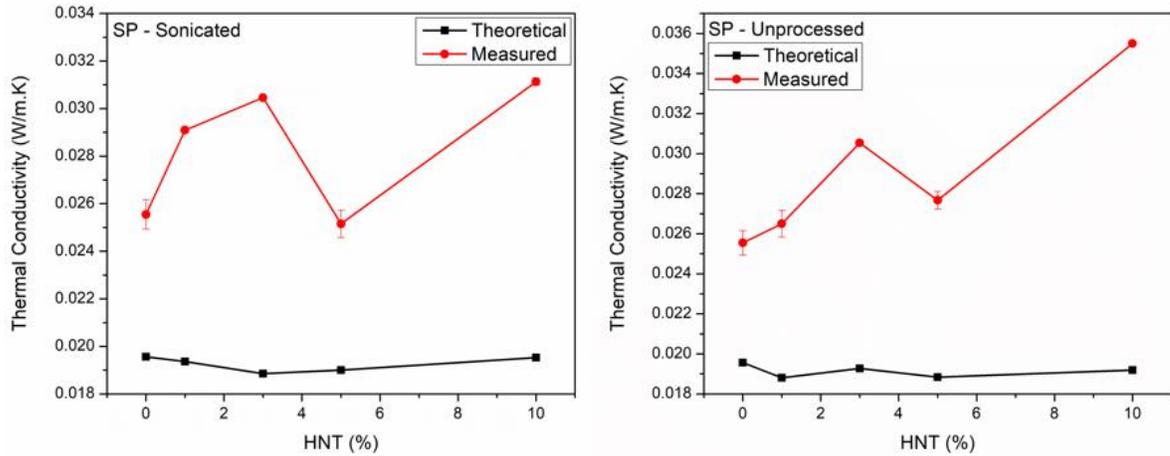
Figure 21. Theoretical and measured thermal conductivity values for SP foams

Nanocomposite B3 and B2 foams were firstly prepared with non-functionalized HNTs, which were only mixed via plenetary mixer with the polyol component. In Figure 22, the SEM images of prepared B3 foams are given. In Table 3, average cell diameter, foam density and thermal conductivity data are presented. From the SEM images, it is observed that with HNT addition the cells became elliptical and at 10% HNT loading they are returning to a circular form. Samples with 10% HNT showed a more rigid structure, cell walls also became more brittle, as some are seen to be ruptured. As the rupturing of the cells is observed, the resulting increase in thermal conductivity is expected, primarily because the opening of the cells contributes to the transfer of heat. In addition to these, the cell size distribution in the samples seem homogeneous, but it broadens after 5% HNT loading. Homogeneous size distribution is important since it is needed to obtain similar thermal conductivity values throughout the foam. It is seen that the thermal conductivity decreases continuously up to 5% HNT loading and slightly increases at 10% loading. Since cell size distributions vary significantly and cell anisotropy is strong, it is not sufficient to explain this behavior by the reduction in cell size.
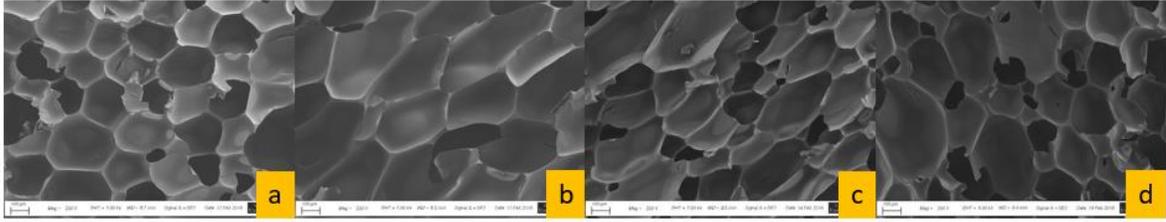
Figure 22. SEM images of B3 foams with HNT-S: (a) reference, (b) 1%, (c) 5%, (d) 10%

In Figure 23 SEM images for B2 foams are given. It should be noted that B2 foam is composed of B3 foam with 15% FR agent, TCPP. It is critical to evaluate the formation and thermal conductivity of these nanocomposite foams in the presence of such FRs. HNT clearly contributes to the formation of smaller cells compared to the reference and compared to its effect in B3 foam. The cell distribution is also more homogeneous compared to the B3 foam. From Table 3 cell size, density and thermal conductivity decrease in a trend, up to 5% HNT loading. This is also consistent with the literature.
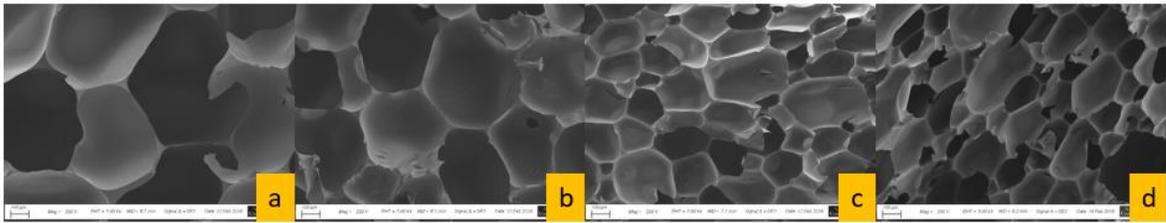
Figure 23. SEM images of B2 foams with HNT-S: (a) reference, (b) 1%, (c) 5%, (d) 10%

Table 3. The change in cell diameter, density and thermal conductivity with HNT for B3 and B2 foams

HNT (%)	Average cell diameter (μm)	Foam density (kg/m³)	Thermal conductivity (W/m.K)
B3 Foam			
Reference	279	90	0.03593 ± 0.0001
1-S	290	85	0.03282 ± 0.0001
5-S	165	78	0.03144 ± 0.0001
10-S	259	81	0.03250 ± 0.0001
B2 Foam			

15% FR (Reference)	596	104	0.04065 ± 0.0001
15% FR + 1-S	507	93	0.03406 ± 0.0001
15% FR + 5-S	322	87	0.03319 ± 0.0001
15% FR + 10-S	211	88	0.03522 ± 0.0001

From Figure 24 it is seen that thermal conductivity follows a similar trend as density in both B3 and B2 foams. B2 foam is seen to have higher thermal conductivity, which was due to the addition of the FR. FRs can cause cell walls to rupture and increase the overall heat transfer thoroughout the foams. Also, both properties are directly proportional to the cell size. Cell rupture observed in 10% HNT loaded foams is again consistent with increasing thermal conductivity. Generally, as cell size gets smaller, density tends to increase, which results in an increase in solid conductivity. Low density may correspond to larger cell size. In this case, even if radiation increases, conduction among the solid foam skeleton can significantly decrease. As mentioned earlier, radiation and solid conduction are interdependent mechanisms. Cell shapes and sizes have a great influence on both of them. The trend in thermal conductivity here can be explained by the balance between these two mechanisms.
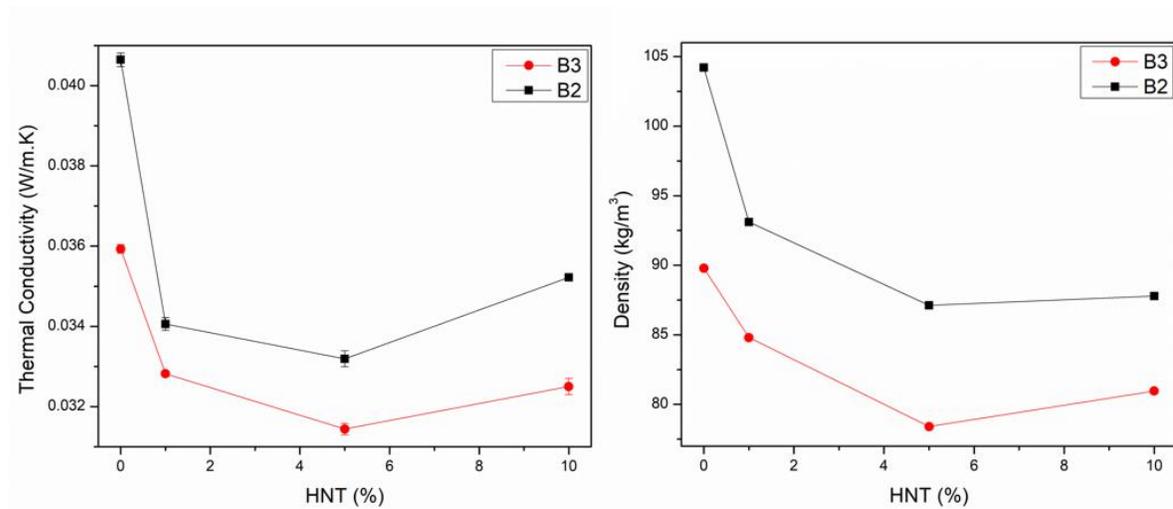
Figure 24. Thermal conductivity and density measurements for B3 and B2 foams

Foam reaction occurs rapidly, so it is significantly affected by the viscosity. Addition of HNT into the mixture certainly increases viscosity. One of the reasons why the cell shapes are different from each other is that the foams are produced "free-rise", which means that they

swell freely in one direction. The density of the foam is also affected by this. The increase in viscosity with HNT addition might have caused the temperature to rise faster during mixing. The fact that temperature rise can cause the blowing agent to pass into the gas phase quickly, but the cells cannot form in such a short time can be another reason for the elliptical cell shape.

In Table 4 viscosity measurements done for B3 and B2 polyols with HNT are given. HNT addition naturally increases the viscosity, but these values are much higher for B3 compared to B2 polyol component. This difference is due to the 15 wt% liquid FR B2 contains. Viscosity reaches to almost 2000 cP at 5% HNT and over 3000 cP with 10% HNT for B3 component. These values are very much undesirable since the reaction time is very short. Additionally, excessive HNT can prevent the foam reaction from taking place properly. Poor reaction will definitely affect the curing and properties. Also, HNTs which already tend to agglomerate may not achieve good dispersion in the matrix. SEM images that are given in Figure 25 belong to 10% HNT loaded samples. The cell size distribution is seen to be quite wide and rupturing of the cell walls is also observed in both samples.

Table 4. The change in the viscosities of B3 and B2 polyol components with HNT addition

HNT (%)	B3 viscosity (cP)	B2 viscosity (cP)
Reference	1148	806
1-S	1095	813
5-S	1965	967
10-S	3121	1627
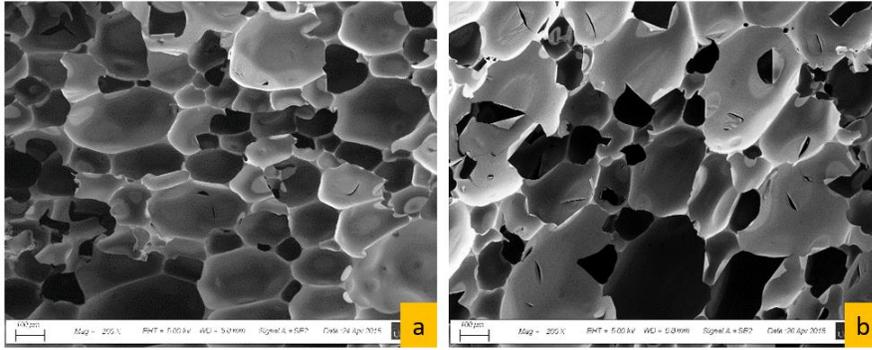
Figure 25. SEM images of B3 and B2 foams with 10% sonicated HNT

3.2.2. Incorporation of FR-loaded HNTs into RPUFs

The loading of HNTs with various active agents under vacuum has been commonly reported in the literature through the filling of HNT lumens and surface adsorption, which will be further detailed in Chapter 4. As shown in Figure 26, the TGA curves of reference HNT and HNT loaded with FR demonstrates that up to 9% loading was achievable.
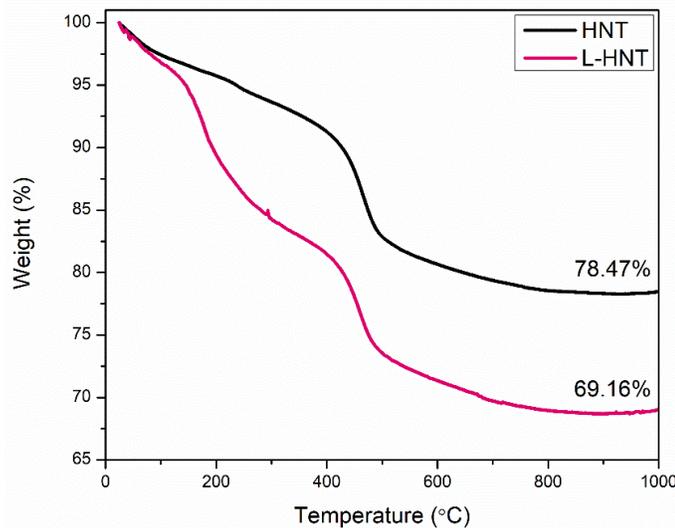
Figure 26. TGA curves for HNT and L-HNT under nitrogen atmosphere

L-HNT was added to B3 foam formulations at 1, 3, 5, 7 and 10 wt% with respect to the polyol component weight. In Figure 27, SEM images of the obtained foams are given. Figure 28 shows the cell size distribution of the six different foams. Table 5 shows the density and thermal conductivity values of the foams. Average cell size was seen to consistently decrease

with HNT addition and the cell shapes are circular in all samples. However, homogeneity of the distribution also decreased which is seen from the SEM images. Following the trend in average cell sizes, thermal conductivity also slightly reduced with increasing HNT. Densities were also seen to decrease. Compared to B3 and B2 foams with unloaded, neat HNTs of which results are presented in the previous section, L-HNTs had minor influence on cell size and cell anisotropy was less pronounced. It can be deduced that the negative effect of the FR on foam morphology can be reduced by loading it into HNT.
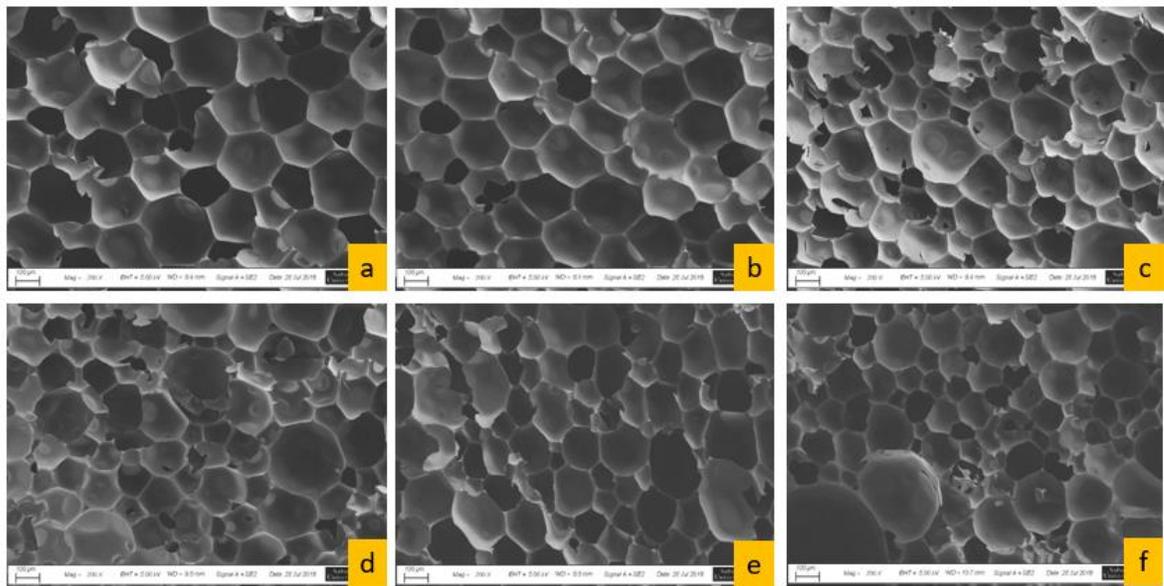
Figure 27. SEM images of B3 foams added with L-HNTs (a) reference (b) 1% (c) 3% (d) 5% (e) 7% (f) 10%
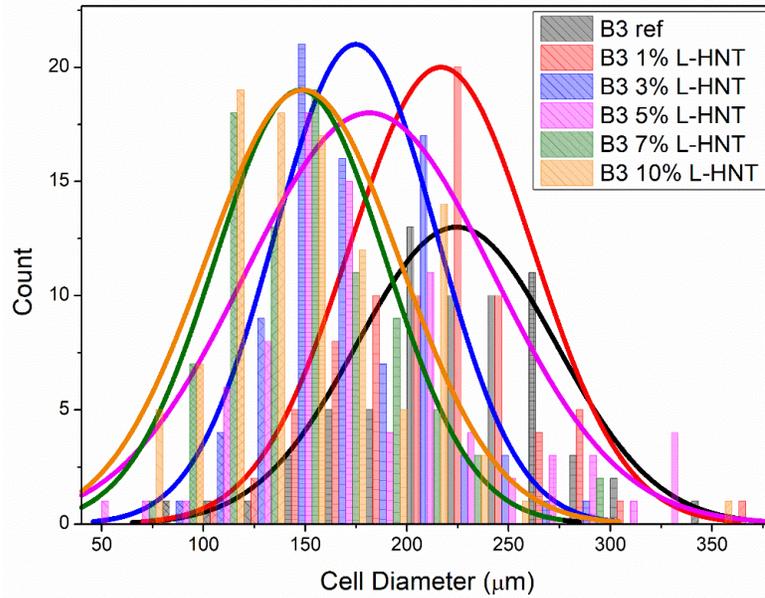
Figure 28. Cell size distribution of B3 foams prepared with L-HNTs

Table 5. Average cell diameters, densities and thermal conductivity values of B3 foams prepared with L-HNTs

Loaded HNT (%)	Average cell diameter (μm)	Foam density (kg/m³)	Thermal conductivity (W/m.K)
Reference	224	74 ± 3	0.0317 ± 0.00065
1	216	80 ± 1	0.0314 ± 0.00031
3	174	77 ± 1	0.0314 ± 0.00033
5	181	76 ± 2	0.0312 ± 0.00021
7	147	75 ± 3	0.0309 ± 0.00007
10	148	72 ± 4	0.0309 ± 0.00006

3.2.3. Functionalization of HNT and B3-HNT-PPO Foams

In order to verify the successful functionalization of HNTs with PPO, FT-IR spectra of reference HNTs and functionalized HNTs were analyzed in Figure 29 along with peak assignments in Table 6.
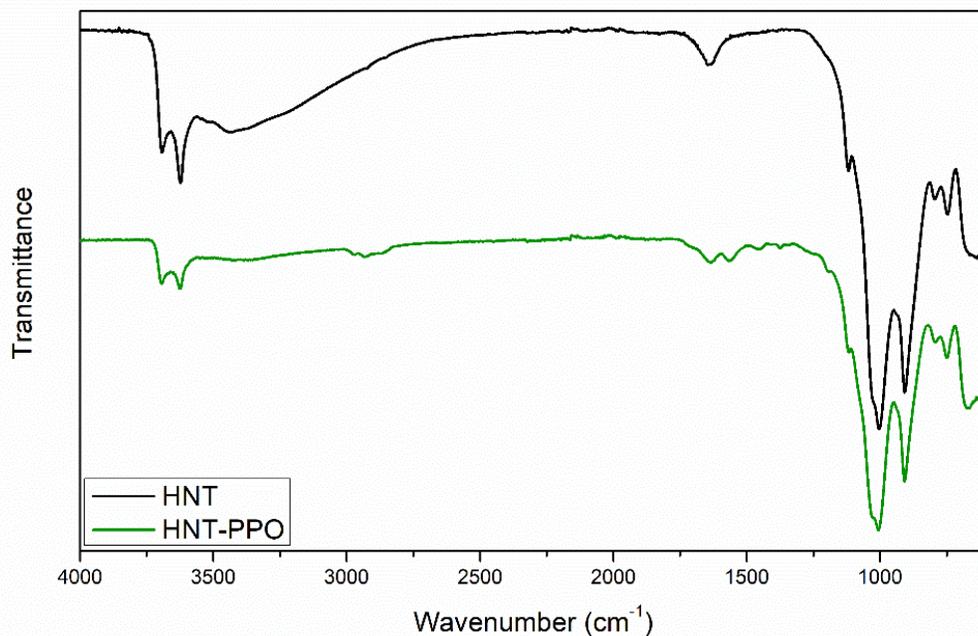
Figure 29. FT-IR spectra of reference HNT and HNT-PPO

Table 6. Peak assignments of FT-IR spectra for HNT and HNT-PPO

	Wavenumber (cm^{-1})	Corresponding peak
Characteristic HNT peaks	3690	O-H stretch of inner-surface hydroxyl groups
	3620	O-H stretch of inner structural hydroxyl groups
	1640	O-H deformation of water
	1120-1000	In-plane stretching of Si-O groups (Si-O-Si and O-Si-O)
	911	Vibration bending of inner hydroxyl groups
	795	Symmetrical bending of Si-O groups
	750	Perpendicular stretching of Si-O groups
HNT-PPO	2970-2870	Symmetric stretching of CH_2 and CH_3 groups
	1564	In-plane bending of N-H groups
	1451	From PPO-polyol – bending vibration of methyl groups
		[41, 62, 72, 75, 76, 107, 108]

TGA curves in Figure 30 also shows a functionalization degree about 9 wt%. Under nitrogen, neat HNT shows a two-step weight loss. Water adsorbed on the surface is lost about 100°C. Above 450°C, structural dehydroxylation occurs. HNT-PPO additionally shows a continuous weight loss between 200-400°C, which is due to the decomposition of grafted species.
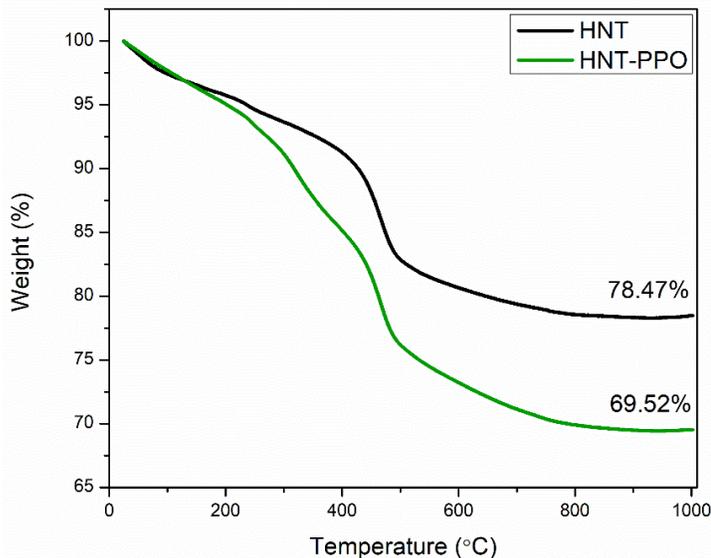
Figure 30. TGA curves for HNT and HNT-PPO under nitrogen atmosphere

Figure 31 shows SEM images of B3 foams containing both HNT-PPO and FR at various ratios, whereas Figure 32 shows the cell size distribution of each foam sample. Primarily, the effect of partially reducing 15 wt% FR in B2 foam and in place, the incorporation of HNT-PPO on the performance of foam samples was investigated. 15 wt% addition of FR into the B3 reference causes an increase both in cell size and the thermal conductivity. Thermal conductivity decreases with further reduction of FR, which is also consistent with the decrease in average cell diameter. In B3-3%HNT-PPO-12%FR sample, cell size is seen to decrease, with respect to both B3 reference and B3-12%FR, however thermal conductivity increases. The reason could be poor mixing ahead of molding, even though ultrasonication is preferred, some re-agglomeration could have taken place. Complex effects between the polyol and the grafted species could also have caused this. Another reason can be the aggressive fracture of the cell walls, as seen in the SEM image, which could cause increased heat transfer.

44
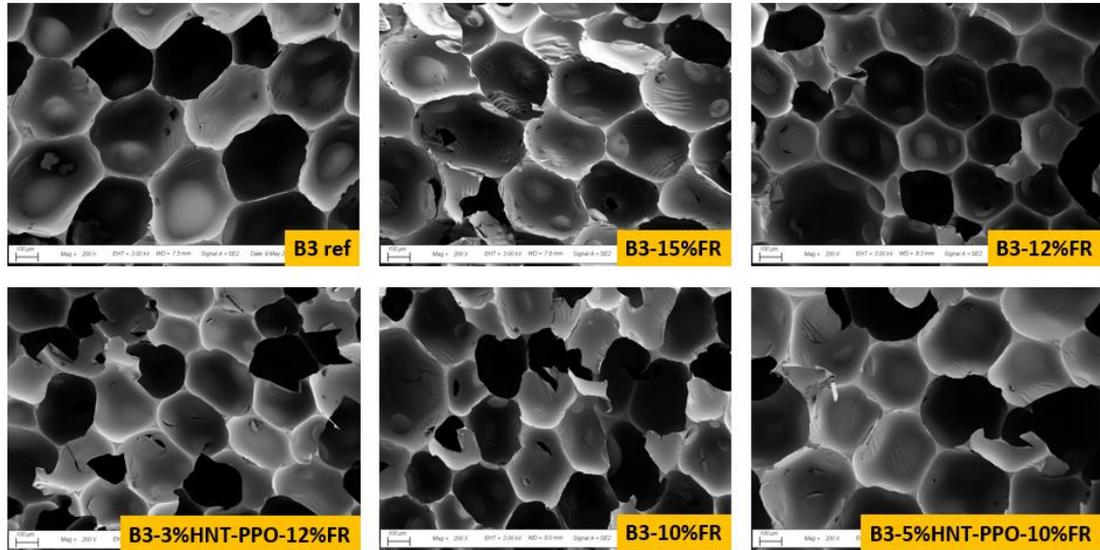
Figure 31. SEM images of B3 foams with HNT-PPO and FR
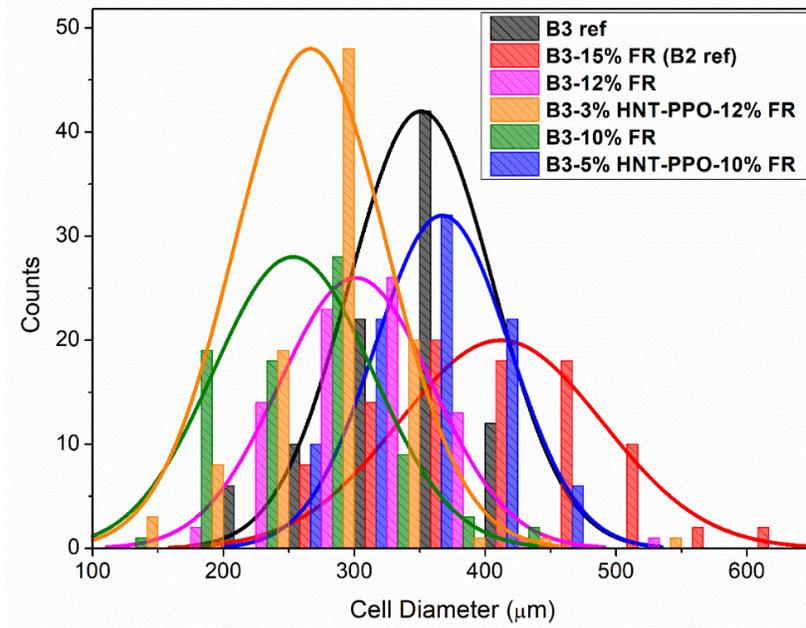
Figure 32. Cell size distribution of B3 foams prepared with HNT-PPO and FR
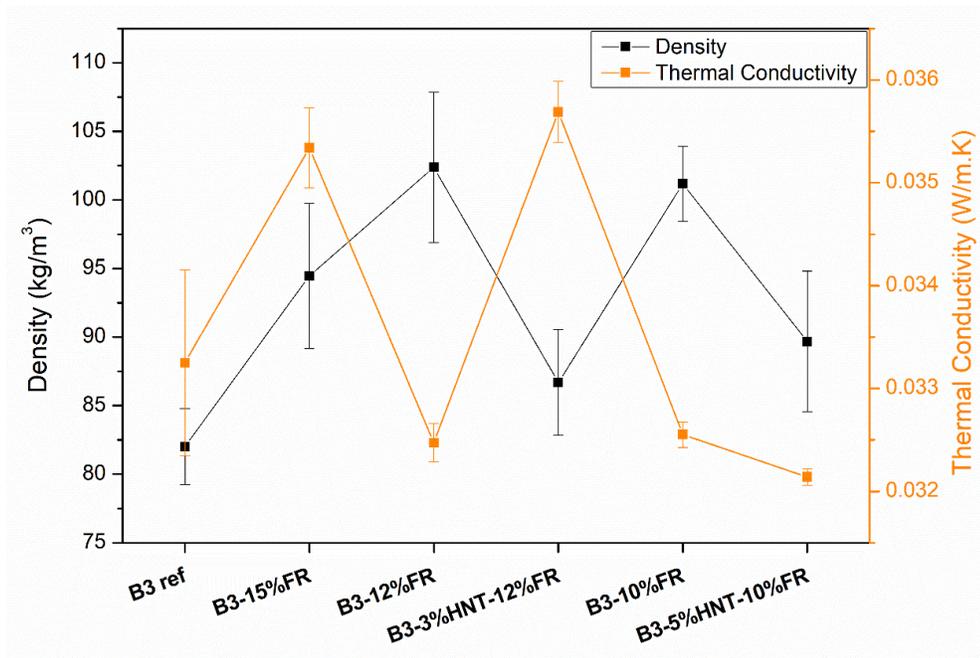
Figure 33. Density and thermal conductivity of samples containing HNT-PPO and FR

3.3. Conclusions

This chapter focused on the thermal insulation performance of HNT-incorporated nanocomposite RPUFs. In this context, firstly untreated HNTs were incorporated into foam various forms of commercially available foam formulations. Results clearly implied inhomogeneous dispersion of the fillers. To improve the dispersion, before mixing with the polyol component, HNTs were treated by probe sonication and grinding. Samples with sonicated HNTs were observed to give narrower cell size distributions, according to SEM measurements. Experimental data did not show very good agreement with theoretical data however, the effect of HNTs could not be considered theoretically, resulting in decreased correlation. In the next step, loading of the FR agent into the lumen and surface of HNTs was carried out in an attempt to partially replace free FR in the foam formulations. TGA characterizations showed that the loading is possible and can reach up to 9 wt%. Average cell size and thermal conductivity were consistently slightly decreased, also density remained about 75±5 from reference sample to 10% HNT loading in the case of L-HNT containing foam samples. This way, the effect of free FR on the cell morphology has been eliminated, such as the opening of the cells, which adversely affects the insulation property. Final part of

this chapter addressed the dispersion quality of HNTs in the foam matrix by their surface modification prior to incorporation. PPO-polyol was covalently attached on the HNT surface with the aid of a silane coupling agent as confirmed by FT-IR and TGA characterizations. Surface functionalized HNT-PPOs were used in combination with the FR agent at various ratios. As a result, there was no significant improvement in thermal insulation property with HNT addition. Also, average cell sizes were observed to be quite high. This suggests that HNT-PPO had a poor distribution in the polyol component and the foam matrix.

In conclusion, in this chapter, it was observed that the cell structure and size of the foams can be significantly influenced by the addition of HNTs and therefore their thermal insulation properties are affected. The addition of unprocessed HNTs into foams generally resulted in inhomogeneous cell size distributions. Sonicated HNTs produced more homogeneous cells. FR-loaded HNTs gave narrower cell size distributions and also, even at 10 wt% L-HNT loading, the thermal conductivity only slightly changed compared to the reference. This may be because some FR is also adsorbed to the HNT surface during the loading process and this surface adsorption may have contributed to the reduction of surface tension in the foam mixture, resulting in better dispersion of the HNTs. Neither the foaming reaction nor foam properties were adversely affected despite the high HNT content. Only FR containing samples showed a trend between the cell size and thermal conductivity, where smallest average cell size provided the lowest thermal conductivity value with the lowest FR content. Yet, possibly due to inhomogeneous dispersion of the fillers, thermal conductivity and average cell size were inconsistent in samples that contained HNT-PPO and FR in combination.

Chapter 4

4. Flammability Tests

4.1. Introduction

4.1.1. Flame Retardancy of RPUFs

Despite their superior insulating and mechanical properties, RPUFs have poor fire resistance. They are easily decomposed and flames can propagate rapidly, specifically arising from foams' high surface area. They have low limiting oxygen index (LOI), typically around 18%, meaning that they cannot extinguish themselves. Also, they release high amounts of gases and smoke. It is important to mention here that the major cause of deaths during fires is the evolution of smoke, together with toxic and asphyxiant gases [86]. Smoke causes reduction in eye sight and makes evacuation harder. These gases evolving from the degradation of the polymer include CO (toxic), CO_2 (asphyxiant), HCN smoke (also toxic) and many others [109]. For this reason, it is of great importance to suppress gas evolution and enhance self-extinguishability of both RPUFs and FPUFs.

PU's low thermal stability and high flammability arises from the biuret, allophanate, urethane and urea groups in its structure. When exposed to flame, biuret and allophanate groups decompose into urea, urethane and diisocyanate, which decompose further [109]. Generally, polyester polyols, specifically those possessing aromatic groups; ring structures, such as isocyanurate which are more easily transformed to crosslinked char systems are desirable in RPUF formulations. Polyisocyanurate foams produce less smoke than PU foams, again because of their ring structure. Isocyanate index and type of catalyst are also said to influence flammability [110]. The density of the foam is important as well, low density sometimes corresponds to easier heat and mass transfer [81].

Poor fire resistance of RPUFs are conventionally enhanced by the use of FRs and there exists a wide variety of FRs used for RPUFs. FRs can be organic materials like halogenated, phosphorus compounds or inorganics such as metal oxides/hydroxides, metal borates. They can be solid/liquid additives or they can be incorporated in the polymer backbone. Liquid FRs may migrate to the surface at high loadings. On the other hand, large amounts of solid FRs may worsen mechanical behavior. Reactive FRs like phosphorus-containing polyols are examples for the latter which do not migrate towards the surface, remaining effective for longer time [111]. Additionally, polymeric/oligomeric species are sometimes preferred over non-polymeric species, since they are more resistant to volatilization, migration and such. [112]. Furthermore, monomers that contain heteroatomic bonds in their structure are known to exhibit better fire resistance because of larger bonding energy, compared to homoatomic bonds [113].

FRs act either or both in the solid (condensed) phase and the gas phase. In the solid phase, firstly they contribute to the formation of a char layer. The char layer has the utmost importance in a fire situation since it prevents heat and mass transfer both into and out of the polymer. As a result, it becomes impossible for the flame to sustain itself and eventually the polymer extinguishes. The thermal stability of the system enhances with a char layer, as also the decomposition activation energy increases [114]. FRs that are active in solid phase also help accelerate the rupture of polymer chains, causing dripping of the polymer. This way, polymer withdraws from the flames. Surely, this sometimes can be an undesirable situation, since flammable drips can cause additional problems by spreading the flame even more [4].

In the gas phase, they are specifically effective in the quenching of flammable H• and OH• radicals which are basically the fuel for the flame [115]. H• and OH• result from the decomposition of the polymer and they sustain the flame. Radicals produced from the decomposition of the FR bond to the radicals and inactivate them. Also, some FRs experience endothermic decomposition around the range of temperatures at which polymer combusts. These FRs absorb the heat released during combustion acting as heat sinks and cool the system. They may also release nonflammable gases like water vapor and CO_2, which has a dilution effect [116]. Figure 34 summarizes the physical and chemical processes taking place during the combustion of polymers.
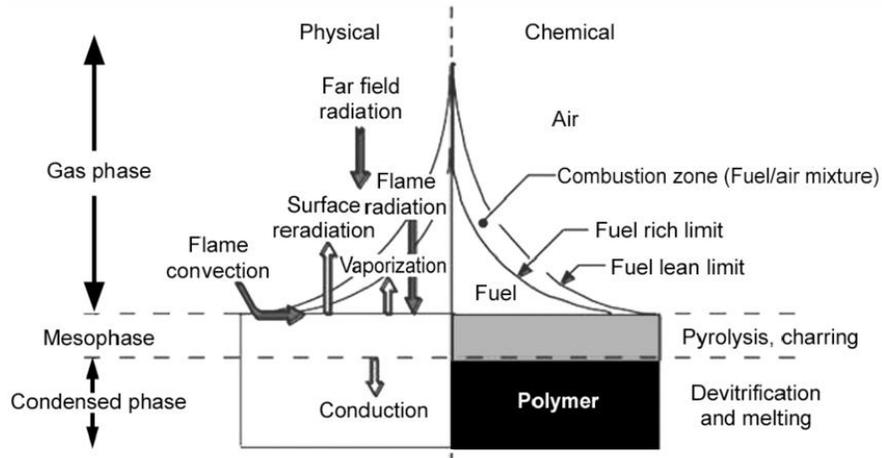
Figure 34. Physical and chemical processes taking place during combustion of polymers [117]

FRs can be divided into several groups with respect to their functions. Different sources claim different number of groups. Palacios et al. [116] mentioned three groups: gas-phase FRs, endothermic FRs and char-forming FRs.

Halogenated FRs, bromine- and chlorine-based FRs are mainly effective in the gas phase. Brominated FRs, especially aromatics used to be highly popular in the past decades and are still used for many applications [118, 119]. Fluorine- and iodine-based compounds are not used, since their decomposition temperatures are either too low or too high than that of many polymers [4]. Halogenated FRs produce Cl• and Br• radicals to scavenge H• and OH• arising from the combustion of the polymer. Figure 35 shows the scavenging mechanism. The main concern related to halogenated FRs is that their decomposition products, halogen acids and metal halides, have persistency in the environment [120]. Also, they produce high amounts of smoke and toxic, corrosive fumes and gases. Zabski et al. [121] have mentioned that halogens can inactivate amine catalysts used in foams. As a result, it is very critical to replace halogenated FRs with alternative, non-hazardous FRs for applications including insulation materials.

$$RX \rightarrow R^\bullet + X^\bullet \qquad X \text{ may be Br or Cl}$$

$$X^\bullet + R'H \rightarrow R'^\bullet + HX$$

$$HX + H^\bullet \rightarrow H_2 + X^\bullet$$

$$HX + OH^\bullet \rightarrow H_2O + X^\bullet$$
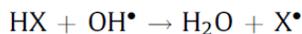
Figure 35. Radical scavenging mechanism of halogen-based FRs [4]

Metal oxides and hydroxides are generally endothermic FRs. Aluminum and magnesium hydroxide are common endothermic FRs. Metal hydroxides decompose to yield a metal oxide, which later takes place in the formation of char layer [4]. It should be noted that HNTs utilized in this study are aluminosilicate-based, natural clays that have the potential to be used as endothermic FRs.

Nitrogen-based FRs are more environmentally friendly and they are also known to evolve less smoke and toxic gases during fire. Most commonly used N-based FRs are melamine and its derivatives [122]. Melamine and derivatives generally decompose endothermically, providing a heat sink effect, in addition to the evolution of ammonia and other inert gases which provides dilution. Ammonia is nonflammable and it is said to dissipate the heat as well. Furthermore, N-based FRs' stable degradation products, namely melam, melem and melon, contribute to the limitation of heat and mass transfer among the char layer [4, 123].

Third group is char-forming FRs. Phosphorus-based FRs are mainly effective in the solid phase, even though some types, like phosphine oxides, show activity in the gas phase as well [124]. Yang et al. [110] claimed that P-based FRs with low oxidation states or low boiling points form $PO_2\bullet$, $PO\bullet$ and $HPO\bullet$ radicals in the gas phase as shown in Figure 36. It was mentioned that these radicals are several times more effective than bromine and chlorine [4]. Phosphorus content may change from 100% to much lower percentages in such FRs and P atom in these compounds can be found in all oxidation states between 0 to +5, though these are not correlated with the efficiency of the FR [125]. P-based FRs produce incombustible gases at high temperatures which are less toxic and corrosive compared to other FR alternatives [112]. Their performance is deeply related to the chemical structure of the polymer. P-based FRs are particularly effective in polymers with high oxygen and nitrogen content like PUs, polyesters, epoxies and such [4, 126].

$$H^* + PO_2^* \rightarrow HOPO$$

$$OH^* + PO_2^* \rightarrow HOPO_2$$

$$HOPO + H^* \rightarrow H_2 + PO_2^*$$

$$HOPO + OH^* \rightarrow H_2O + PO_2^*$$

$$HOPO_2 + H^* \rightarrow H_2O + PO_2^*$$
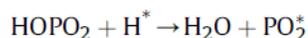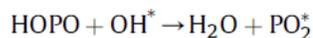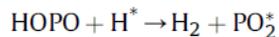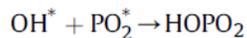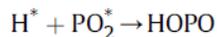
Figure 36. Radical scavenging mechanism of phosphorus-based FRs [127]

P-based FRs alter the thermal degradation pathway of the RPUFs by an acid catalysis effect on urethane bond degradation and promoting carbonization [127, 128]. The mechanism can be seen in Figure 37. In the condensed phase, P-based FRs start decomposing earlier than the PU polymer and they produce phosphoric or polyphosphoric acids. These acids give reaction with the polymer to catalyze their dehydration reaction and char formation. It was also previously reported that phosphoric acid reacts effectively with carbodiimide, which is formed from the condensation of the isocyanate. This reaction contributes to the formation of a crosslinked, carbonaceous char layer [109]. P-based FRs may create a P-C char from reactions of organic components or a glass-like one derived from polyphosphoric acid [115]. The crosslinked char layer insulates the polymer and decrease propagation of the flame and smoke release and prevent dripping. Self-extinguishability of the system increases substantially [129].
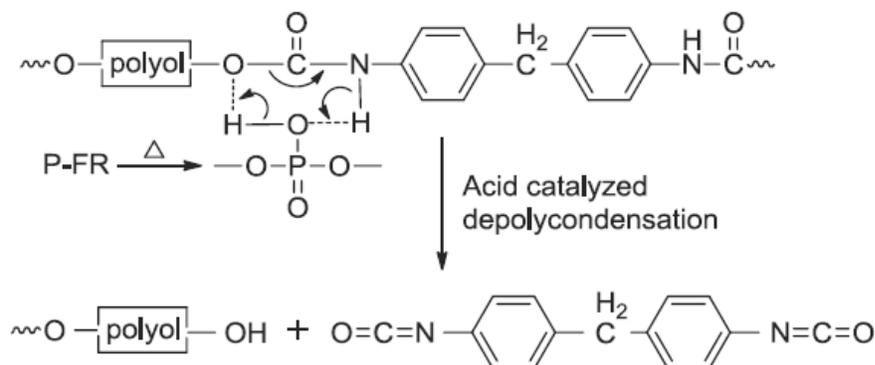
Figure 37. Acid catalysis effect of P-FR on urethane bond degradation [127]

A specific group of FRs, intumescent FRs (IFRs), can also be included under char-formers

group. These were originally developed for use in fabrics, wood and coatings [4]. Intumescent systems start to char and expand to form a cellular char when they are exposed to flame or heat above a certain temperature. These systems consist of three parts: acid source, carbon source and foaming (blowing) agent. Acid source sort of behaves like a catalyst, this is usually an inorganic acid or an acid salt which supports the dehydration of the carbon source. Carbon sources are usually carbohydrates. Polyols can sometimes be recognized as carbonizing agents. In addition, the number of carbon atoms controls the amount of char to be produced. The acid has to be activated below the decomposition temperature of the carbon source, consequently, the dehydration reaction has to be taking place around polymer decomposition [4]. Foaming agents decompose to evolve gases which expand the polymer to yield a foamed char. Expandable graphite is commonly used for this purpose. Ammonium polyphosphate (APP) is also a common agent in such systems, sometimes serving as both the acid source and the blowing agent. APP, pentaerythritol and melamine form one of the most commonly used IFR systems [130, 131]. IFRs are common in the polypropylene flame retardancy literature [132, 133].

Sittisart et al. [134] suggested one another group, synergists. Some materials can show a combined synergistic effect for flame retardancy. This can occur in two ways: the material is not a FR but can work with FRs, improving their performance or two or more FRs work together to improve total flame resistance. Solid-liquid compounded FR systems help controlling the viscosity of the polymer matrix and can decrease the FR amount used, sometimes providing even better flame retardancy than they were used alone [135].

Phosphorus can have a synergistic effect on flame retardancy with nitrogen [122]. It was studied in the past that polymers with both P and N possess good thermal properties and flame retardancy, in addition to observable self-extinguishability [112, 136]. In addition to heat sink and dilution effects coming from nitrogen, if the system has P-compounds, its condensation products can also take place in the crosslinking of phosphorus acid to form P-C char [137].

Yang et al. [110] used APP as a solid phase and dimethyl methyl phosphonate (DMMP) as a gas phase FR for polyisocyanurate-PU foams. Slight increase in thermal conductivity was observed, on the other hand, all samples containing APP and DMMP at different weight

percentages obtained V-0 rating in vertical burning test and their LOIs reached over 30%, from 23% for neat PIR-PUR sample. However, peak heat release rate (pHRR) showed an increase and only a small change was observed in total heat released (THR).

Singh et al. [109] prepared a FR by reacting phosphoric acid, formaldehyde, melamine and urea (PMUF). RPUF samples were impregnated with an aqueous solution of this mixture for different concentrations and impregnation times. Burning rate and burnt length decreased, LOI changed from 18% to 24% with increasing PMUF concentration. PMUF-RPUFs exhibited less and delayed smoke production as well.

Zhang et al. [138] synthesized 9,10-dihydro-9-oxa-10-phosphaphenanthrene-10-oxide (DOPO)- and n-benzylideneaniline (BA)-based FR, getting use of the aromatic structures for enhanced flame retardancy in RPUFs. At 20 php loading of DOPO-BA, a slight decrease of 11 kW/m^2, in pHRR was measured. Total smoke release (TSR), changed from 355 M^2/m^2 to 185 M^2/m^2, which is probably due to the formation of a strong char. Yet, with addition of more FR, slight increase in thermal conductivity was observed - closed cell ratio decreased. It is known that the amount of FR additives is important since they can cause cell opening, which facilitates heat transfer [81, 110].

Xu et al. [5] made APP- and DMMP-incorporated RPUF composites using three different nano additives, MMT, zeolite and zinc oxide. Significant change in the structure of the char was observed with nanoparticles. Zeolite-incorporated foams had lower smoke production rates (SPR), due to zeolite's porous structure, which holds volatiles. However, MMT has shown great increase in viscosity at 5 wt% loading, impeding the foam reaction.

Thirumal et al. [122] compared melamine polyphosphate (MPP) and melamine cyanurate (MC) as FRs in RPUF. Deterioration in mechanical properties was observed with MPP addition, however, flame retardancy enhanced, compared to MC-added foams, due to the synergistic interaction of P and N.

Chlorinated phosphorus FRs such as TCPP, tris(2-chloroethyl) phosphate and derivatives are common in both FPUFs and RPUFs. The use of these are limited due to potential toxicity, bioaccumulation and environmental risks [127]. TCPP is listed among the mostly used chlorinated organophosphorus FRs, almost accounting for 80% of the chlorinated FR market

54

in Europe according to previous reports. It is an additive-type FR, it does not give any chemical reaction with foam components. Because of this, through leaching, volatilization and direct contact etc. it is liberated into the environment [139, 140]. TCPP can be added in much lower quantities than melamine to be effective, it is sometimes used in combination with melamine as well. It is claimed to act both in gas and condensed phase, through the formation of HCl and phosphoric acid and derivatives, respectively [141].

Xu et al. [135] prepared RPUFs incorporated with TCPP and phosphoric acid-modified aramid fiber (MAF). Enhancement in the regularity of the RPUF cellular structure was observed, in addition to an increase in LOI by 39.2% and a decrease in pHRR by 59.6% and TSR by 26.7%, with addition of TCPP and MAF together. Charred residues showed dense, compact structures, indicating strong barrier and reinforcing effect from MAF. TCPP enables the quenching of H• and OH• radicals by PO• and Cl• radicals, as it also contributes to the formation of the char layer which is composed of P-O-C linkages, from the reaction of MAF and polyol.

4.1.2. Flame Retardancy of HNTs

In polymer-clay nanocomposites, flame retandancy is usually attributed to barrier effects. During combustion, clay particles migrate to the surface, forming an inorganic-rich char layer. It is also emphasized in the literature that clay particles mechanically reinforce the char layer, due to their high stiffnesses. Certainly, there is a threshold for clay addition. Too much clay loading may antagonistically affect the flame retardancy, as it is also problematic for the polymerization [120]. Clay particles are highly thermally stable as well, as for HNT, it is stable up to 450°C and generally has a residue about 85 wt% at 800°C [7].

HNT is effective by several mechanisms for flame retardancy. First of all, it greatly contributes to formation of an integrated char layer and mechanically reinforces it. During the formation of this layer, HNT can also act as a physical, impermeable barrier for vapors and gases (even though this would be more accurate for plate-like particles). On the other hand, HNT can also entrap degradation products in its lumen, this has been thought to be an important mechanism [7]. The dispersion of nanoparticles is again influential here, since it determines the efficiency of this mechanism. Surely if the lumen is filled, this might not take

place. Additionally, above 450°C, HNT transforms into metakaolin due to the degradation of interlayer aluminum oxide. This endothermic reaction results in the release of 15 wt% water, which drives heat away from the system and may also have a dilution effect. Interestingly, Lecouvet et al. [120] showed through NMR that HNT has formed Al-O-P bonds above 500°C with APP and/or its decomposition products, helping further stabilize the phospho-carbonaceous char layer. Furthermore, there may be a small contribution to flame retardancy coming from iron contamination, namely, Fe_2O_3. It can entrap free radicals from the degradation reaction very efficiently [7, 55]. Naturally, Al and Si atoms of HNT can be replaced by Fe, Cr, Ti etc. atoms, amount depending on the deposit. Iron oxide is the most frequent contamination, sometimes accounting for up to 3 wt% [142]. It was also mentioned that HNT is useful for intumescent formulations due to its complex pore structure and hydroxyl groups on its surface, which makes some molecules to be more easily adsorbed [143].

HNT and other clays are used in flame retardant formulations for a wide range of polymers, including PU [5, 144], polyethylene [145], polyethersulfone [146], poly vinyl chloride [147], polypropylene [148, 149], polyamide [150], epoxy [151] and many others. Earlier studies about RPUF-clay nanocomposites for flame retardancy are usually with MMT. Differently from HNT, it is a layered clay, so it needs to be exfoliated for good dispersion in matrices.

Marney et al. [152] have studied the flammability of Nylon 6/HNT composites. Nylon 6, a polyamide, has quite good flame resistance with an LOI degree about 21-25%, however, it exhibits serious flammable dripping. With the aim of eliminating this problem, the group prepared samples with HNT amount changing from 0 to 30%. THR, pHRR and char residue consistently decreased with increasing HNT loading. It was understood that the char layer got stronger. LOI increased up to 30% at 30% HNT loading. On the other hand, HNT had a very small effect on CO and CO_2 evolution. An increase in the smoke production was observed with HNT addition but was independent of HNT amount, which is probably due to some physico-chemical interactions between HNT and the polymer. Another conclusion drawn is that HNT is effective in the condensed phase of the burning media.

It is emphasized in the literature that usually HNT itself alone is not enough to provide significant improvement in flame retardancy. Even if that is the case, it requires high loading,

up to 30 wt% and maybe more. This loading amount may be extremely high for some polymers, as it will greatly influence viscosity and hinder polymerization reactions. This includes rigid foams as well. For this reason, in some studies conventional FRs are partially replaced with clay particles to get a synergistic effect. HNTs have also been used as part of IFR systems. To be effective, IFRs generally have to be added in large amounts, however they are known to deteorite the mechanical strength of polymers. To overcome this, they are sometimes paired with clay nanoparticles [153, 154]. As a result, by combining HNTs with FRs it is still possible to get exceptional flame retardancy while using less potentially harmful FR compounds.

Lecouvet et al. [120] have an extensive study on such a nanocomposite. They produced polypropylene (PP) samples containing an IFR system and HNT at determined amounts. IFR system consisted of an APP derivative coated with a nitrogen-carbon containing compound. Apart from the neat PP, four different samples were prepared fixed at 20 wt% FR, but with different ratios of IFR and HNT. Cone calorimeter results showed a decrease in $pHRR_1$ from 631 kW/m^2 for neat PP to 127 kW/m^2 and less for composites. This decrease indicates the formation of a char layer. Also, time to reach $pHRR_2$ was seen to increase for increasing amount of HNT due to the enhanced char. At 1.5 wt% HNT, samples gave a V-0 rating in UL-94 test vertical burning test, where neat PP exhibited serious melt dripping. When only IFR was used at 20 wt%, it left a severely cracked, discontinuous char and also side shrinkage was observed after 480°C, about when char layer starts to degrade. In reference and IFR-only samples, morphology of the char was seen to be highly porous which makes heat and mass transfer easier. HNT provided a smoother and denser layer with less shrinkage. Thanks to their high aspect ratios, HNTs impeded the growth and liberation of gas bubbles from the char and reduced convective-radiative heat transfer through the char layer. These point out the reinforcing effect of HNTs as well.

The loading of various agents into HNT via vacuum cyclization is a common approach, as briefly mentioned in Chapter 1. Via this approach, the loading of FR agents into HNTs has also been reported in the literature. Joshi et al. [155] loaded triphenyl phosphate (TPP) by 4 wt% efficiency in HNT and used it in a latex coating. TPP-loaded HNTs did not improve the flame retardant property of the coatings, however, 5% neat HNT addition proved to be better

than 5% FR addition. Yah et al. [67] showed the hydrophobization of the inner surface of HNT by modification with octadecylphosphonic acid. Then, Jing et al. [156] loaded such modified HNT with a common FR, bisphenol A bis(diphenyl phosphate) (BDP). Release behavior was studied with UV spectroscopy to show that surface-modified HNT can hold threefold more BDP than neat HNT.

Marney et al. [157] intercalated HNTs with phenyl phosphonic acid through covalent bond formation, and incorporated these into polyamide 6 (PA6) matrix for use as FR agents. Intercalation was confirmed by TGA and XRD analyses. At 10% unmodified HNT loading, pHRR dropped from 1890 kW/m^2 to 1296 kW/m^2, whereas the addition of PPA-HNT decreased this value to 844 kW/m^2. 10% PPA-HNT also changed the shape of heat release rate (HRR) curve, indicating that after a critical concentration of PPA, HNT and PPA can interact to show a synergistic effect altering the degradation pathway. However, CO production of this nanocomposite was three times higher than that of the reference PA6. Smoke production was also significantly higher. It was stated that the HNTs greatly contributed to the development of a very strong char layer, under which the polymer heated up and reacted with small chain pyrolysis products for a long period until there was enough pressure to break the char.

Zheng et al. [158] loaded DMMP in HNTs in order to get rid of the plasticizing effect of organophosphorus FR on epoxy. Loading efficiency was found to be 24.2 wt%. Fluorometer analysis showed that DMMP was released in two stages, which were attributed to the release of FR adsorbed on HNT surface and that was loaded into the lumen respectively. HNT-DMMP addition to epoxy resin helped to significantly decrease HRR, THR, TSP, CO production rate and mass loss rate (MLR). Residues after cone calorimeter tests showed compact, nonporous char layers for samples with HNT-DMMP, whereas the reference epoxy produced a porous char. It was concluded that HNTs can act as physical barriers to prevent heat and mass transfer, suppress smoke release through the release of hydrate water and entrap degradation products. Also, rapid gasification of DMMP provided the formation of polyphosphoric species to contribute to the char layer.

Boonkongkaew et al. [159] also studied the plasticizing effect of organophosphorus FRs on PA6. The group loaded BDP into HNTs and achieved a loading of 16.5 wt%. Loaded HNTs

or unloaded HNTs and BDP were added to the PA6 polymer both together and separately in different combinations. While directly added BDP was effective in the early stages of burning, prolonged release of the loaded-BDP was observed during cone calorimeter tests. Addition of HNT and BDP separately at different ratios helped to decrease the HRR and THR of the polymer, however combined incorporation of unloaded/loaded HNTs with the FR showed a synergistic effect to give even decreased HRR and THR values from about 800 kW/m^2 to 500 kW/m^2. BDP's plasticizing effect on the composites was also significantly reduced through loading it in HNTs.

Apart from simple one-shot free-rise method, there are some interesting approaches as well. Smith et al. [160] have prepared aqueous suspensions of 0.5 wt% HNT in branched polyethyleneimine and in poly(acrylic acid), then coated these on FPUF samples via layer-by-layer technique. TGA results showed a difference in residue of about 20% between neat PU and 5-bilayer coated PU both under oxygen and nitrogen, and a great reduction in pHRR and TSR was observed.

4.2. Results and Discussion

4.2.1. Preliminary Flame Tests of RPUFs

SP foam samples containing 0, 1, 5 and 10 wt% HNTs were tested with the small flame test setup as seen in Figure 38. In all samples, ignition occurred during application of the flame. Flame extinguished just as the flame was withdrawn and therefore could not reach the 150 mm threshold. In addition, flashing and blazing was observed during the test, which are undesirable phenomena. Flame height reached 110-120 mm in 1% samples, 90-100 mm in 5% samples and 120-130 mm in 10% samples. This value being the highest for 10% HNT loaded samples may be related to the changes in the morphology of the foams. It is also seen that the flame was only effective on the surface of samples. This might be pointing out the barrier effect of HNTs as it also highlights the ability of the foam formulation to provide a durable char.

Figure 38. 1% HNT loaded SP foam samples after testing with small flame test

From the tests that were done with our setup, it was seen that SP foam has better flame resistance than DEC foam. All SP foam samples immediately formed a strong char layer upon flame application and as soon as the flame was taken away, samples extinguished. Cross sections of burned samples showed no penetration of flame inside the samples. In addition to these observations, chemical characterizations of SP polyol component showed presence of aromatic structures, which are known to be effective in flame retardancy. No significant difference was observed in these results by the flame test of SP foam samples in relation to HNT amount. Tested samples can be seen in Figure 39.

Again, char layer was quickly formed on the surface of DEC foam samples as soon as the flame was contacted. When the cross sections of the samples were observed after testing, the flame was seen to be only effective on the outer surface as it could not reach into the foam core, as seen in Figure 39 (b). Differently from SP foam samples, DEC foam samples sustained burning for 10-25 seconds longer after the flame was taken away and then extinguished themselves. Also, as given in Table 7, this period decreased with increasing HNT amount. Additionally, in both types of foams, gas and smoke release in high amounts and sometimes black, particulate matter were observed in the smoke.

Figure 39. Tested (a) SP (b) DEC foam samples and on the right-side of the images, cross sections of the reference samples

Table 7. The change in average extinguishment time with HNT amount for DEC foam

HNT (%)	Average extinguishment time (s)
Reference	22
1-S	25
3-S	22
5-S	12
10-S	10

4.2.2. Preliminary Flame Tests of RPUFs with Sonicated HNTs

All B3 foam samples, which had no FR, ignited during the application of the flame and flames passed the 150 mm limit. Samples sustained burning even when the flame source was moved away. They all formed char layer but created no flaming drips. As given in Table 8, time to exceed the 150 mm limit was measured to be 10, 11, 8 and 10 seconds with increasing HNT

amount. Given the proximity of the durations, these results are insufficient to explain the effect of HNTs on the flame resistance of foams.

In B2 foam, which contains 15% FR, the effect of HNT to flame retardancy was also unclear. All samples were ignited as they contacted the flame source and the flame grew but did not reach the 150 mm limit. Char layer was formed on surface, also no flaming dripping was observed. From the images in Figure 40, it is clear that B2 foam has better flame retardancy than B3 reference foam.

Table 8. Small flame test results for B2 and B3 foams

HNT (%)	Ignition	Reaching 150 mm limit	Time to exceed 150 mm limit (s)	Burning of filter paper
B3				
Reference	Yes	Yes	10	Yes
1-S	Yes	Yes	11	Yes
5-S	Yes	Yes	8	Yes
10-S	Yes	Yes	10	Yes
B2				
Reference	Yes	No	-	No
1-S	Yes	No	-	No
5-S	Yes	No	-	No
10-S	Yes	No	-	No
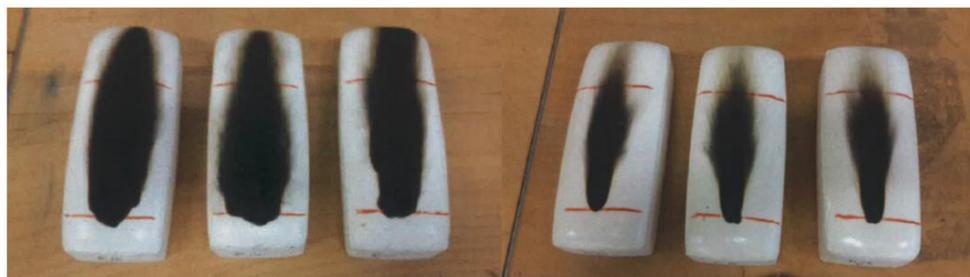
Figure 40. 10% HNT loaded B3 and B2 foam samples after small flame test

4.2.3. Flame Retardancy of RPUFs with Functionalized HNTs and FR Agent

LOI describes the minimum level of oxygen required for the flame to sustain itself. Generally, materials that possess LOI over 21% are considered to be "self-extinguishing" [4]. LOI does not give conclusive results about the flammability of the materials but rather it gives an insight and can be used for ranking/comparing them. In Table 9 LOI results for foams containing HNT-PPO and FR are presented. It is clear that the reference foam is highly flammable, with an LOI of 17%. With the addition of FR, LOI reaches 22%. However, these results are insufficient to explain the effect of HNT. It is seen that the increased oxygen index arises from the FR itself.

Table 9. Limiting oxygen indices of B3 foams containing HNT-PPO and FR

Samples	Oxygen index (%)
B3 reference	17.0
B2 ref (i.e. B3-15%FR)	22.0
B3-12%FR	22.2
B3-3%HNT-PPO-12%FR	21.0
B3-10%FR	22.0
B3-5%HNT-PPO-10%FR	22.0

Smoke is an important parameter in the event of a fire, since it is toxic and also makes evacuation harder. As mentioned earlier in this chapter, most of the deaths in fires occur due to smoke. Smoke density measurements give insight about real fire situations. In the testing chamber, there is a continuous beam of light. As the material burns inside the chamber and produces smoke, how much of the light is transmitted across the chamber is measured continuously and translated into specific optical density, a unitless parameter, as the output. Higher optical density corresponds to higher smoke production [79].

In Table 10, maximum specific optical densities (D_s max) of the foam samples are given. As FR amount is decreased, more smoke is produced. D_s max changes from 230 for 15% FR to 330 for 10% FR. Also, both B3 and B2 reference foams show close D_s max values, where

B2 apparently produces higher smoke. However, with HNT addition D_s max goes up to 370, indicating poor barrier effect from HNT. It clearly cannot act as a smoke suppressant up to a loading of 5%.

Table 10. Maximum specific optical densities of B3 foams containing HNT-PPO and FR

Samples	D_s max
B3 reference	221 ± 4
B2 ref (i.e. B3-15%FR)	231 ± 36
B3-12%FR	283 ± 21
B3-3%HNT-PPO-12%FR	370 ± 6
B3-10%FR	330 ± 15
B3-5%HNT-PPO-10%FR	343 ± 11

In Table 11, time to ignition (TTI), peak heat release rate (pHRR), total heat released (THR), average specific extinction area (SEA), average mass loss rate (MLR) and residual mass data of the tested foam samples are given.

When exposed to fire, the polymer is heated above its decomposition temperature at some point and ignites. This is described by TTI. It can be correlated to the ease of igniting the material [79]. With FR and HNT addition, TTIs of the samples were longer. HNT-PPO containing foam samples also showed slightly higher TTI values than FR-only samples. FR induces surface charring as soon as the flame is contacted, so it is expected to take a longer time for the char to break and burning to start. The ignition of polymers can be influenced by changes in thermophysical properties and degradation pathway through the incorporation of nanofillers such as HNTs in this case. However, it should be noted that TTI is affected by several mechanisms against each other [146].

Figure 41 shows the HRR profiles of B3-based HNT-PPO and/or FR containing foam samples. Heat release rate describes the thermal energy produced during the combustion of the material. It simply determines the fire behavior of the burning material. pHRR could be recognized as the maximum flammability of the material and higher pHRR means that a more

violent combustion is taking place. HRR is also correlated to or determines other flammability properties of the materials like smoke generation [79]. The neat B3 foam shows a pHRR of 410 kW/m^2 and the samples burn almost completely in three minutes. FR addition significantly decreases pHRR values. On the other hand, HNTs did not have a significant effect on the pHRR's, which were seen to be comparable to that of containing FR only. Also, B3 and B2 reference samples did not show a second peak heat release, showing that the char layer stayed intact. Yet, HNT-loaded samples show a very small peak about the second minute of testing. Eye inspection also supported this. In Figure 42 optical photographs of the samples are given. As seen, reference samples had continuous char layers with no visible cracks. However, in HNT-loaded samples the char formed on the surface was detached from the sides to expose the inner polymer to flames. This is attributed to the pressure of formed gases under the char to bursting the layer. THR decreases by 20% with FR addition but starts to increase with increasing HNT amount. Higher THR means more heat release during burning, therefore it also indicates possibility of secondary fire. Average MLR values showed an increase for all samples compared to the reference, which should be related to the flame retardancy mechanism of the FR.

SEA describes the smokiness of fuels. Higher SEA means higher amount of smoke being emitted per kilogram of the fuel [79]. From Table 11, SEA is seen to significantly increase with FR addition, but with 5% HNT-PPO it is reduced to a value even under than that of the reference B3. This is most probably due to the adsorption of volatiles by HNTs. High SEA for FR-only samples should be because of the FR's activity in the gas phase, producing radicals. Also, primary pyrolysis gases may undergo secondary pyrolysis reactions, which can increase the smoke. It can be deduced that the FR also greatly contributes to the smoke production. Residues after burning increased by 10% with FR and HNT addition as well.

Table 11. Cone calorimeter results of B3 foams containing HNT-PPO and FR

Samples	TTI (s)	pHRR (kW/m²)	THR (kW/m²)	Avg MLR (g/m²s)	Avg SEA (m²/kg)	Residue (%)
B3 reference	3.00±0.25	410±18	38.8±1.5	8.5±1.6	674.8±9.6	15.83±0.62
B2 ref (i.e. B3-15%FR)	6.00±1.25	267±37	27.5±0.5	10.9±3.1	932.2±121.1	28.75±1.49
B3-12%FR	7.25±0.25	280±17	34.5±4.1	12.2±0.3	652.1±69.0	25.72±1.09
B3-3%HNT-PPO-12%FR	7.50±1.12	263±14	30.5±0.8	11.4±0.4	733.0±107.9	27.37±0.49
B3-10%FR	6.60±0.38	254±10	33.1±0.6	11.1±1.1	561.0±27.1	25.57±0.18
B3-5%HNT-PPO-10%FR	7.75±0.25	253±13	32.1±0.7	11.4±1.1	634.1±52.9	26.54±1.08
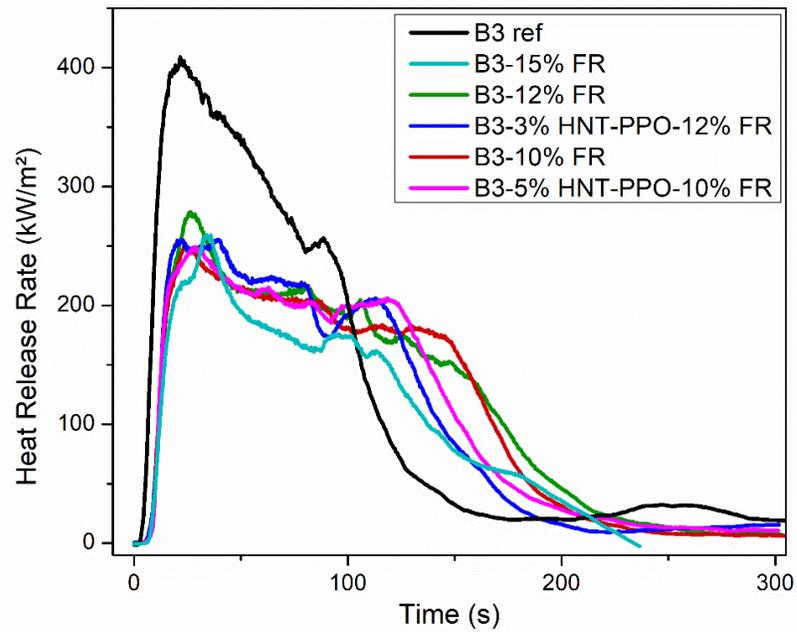
Figure 41. Heat release rate profiles of the samples
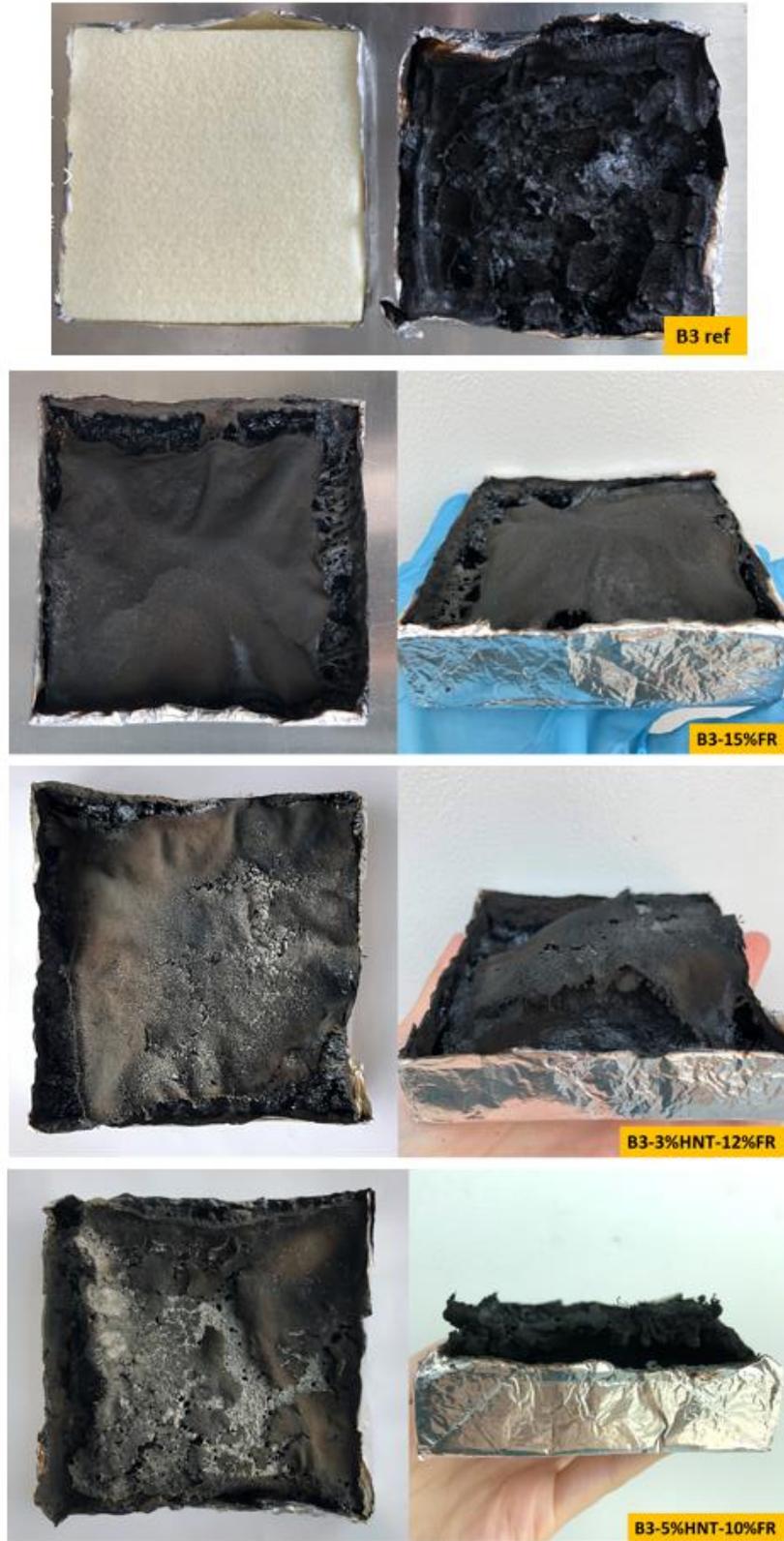
Figure 42. Appearance of some samples after testing with cone calorimeter

Post ignition smoke production and average SEA were also consistent. Results in Table 12 showed that FR addition increases smoke production per unit area, which later decrease with HNT addition. Such an increase is probably due to the FR's action in the vapor phase. Halogen and/or phosphorus radicals produced by the decomposition of FR may contribute to the formation of higher smoke compared to neat reference. CO and smoke are produced because of incomplete burning, the amount of these depend on the material's properties and the intensity of fire. CO yield increased with increased HNT amount, indicating increased toxicity of the smoke. Samples are burning rather efficiently. CO_2 yield decreases with HNT and FR, however it decreases even more with only FR. CO production is proportional to HNT amount, but CO_2 production is not. Oxidation of CO is important, since it is the main heat source in combustion of polymers.

Table 12. Cone calorimeter results of B3 foams containing HNT-PPO and FR

Samples	Post-ignition smoke production (m²/m²)	CO yield (kg/kg)	CO_2 yield (kg/kg)
B3 reference	1108.8±40.5	0.086±0.001	2.84±0.08
B2 ref (i.e. B3-15%FR)	1412.1±190.7	0.095±0.005	1.56±0.08
B3-12%FR	1246.1±252.2	0.148±0.004	1.99±0.99
B3-3%HNT-PPO-12%FR	1157.8±156.2	0.142±0.018	2.37±0.17
B3-10%FR	1048.9±21.6	0.146±0.009	2.06±0.11
B3-5%HNT-PPO-10%FR	1103.0±114.7	0.147±0.006	2.21±0.03

4.2.4. Flame Retardancy of RPUFs with FR-loaded HNTs

HNTs loaded with the halogenated FR were incorporated into B3 foam formulation by 7% and 10%. In Figure 43 heat release rate profiles of these two samples are given along with heat release rates of B3 foam samples containing HNTs and FR mixtures from Section 4.2.3 for comparison purposes. B3-7%L-HNT sample follows a similar behavior as B2 reference, which contains 15% free FR. However, pHRR value for this sample is 228 kW/m², which is considerably lower than that of the B2 reference. B3-10%L-HNT showed a further decrease

68

in pHRR, reaching 200 kW/m^2, providing the lowest pHRR among all the samples. THR values for both samples, given in Table 13, are well below the B3 reference, B3-7%L-HNT is almost the same as B2 reference and B3-10%L-HNT is even lower. From Section 4.2.3 all FR containing samples showed increased average MLR values, which were attributed to the halogenated FR's flame retardation activity. However, B3-7%L-HNT and B3-10%L-HNT samples showed average MLRs comparable to that of B3 reference, which indicates L-HNT does not have an effect on MLR. Loading the FR into the HNTs clearly helped to reduce the negative effect of the FR on mass loss. Residual mass increased to 33% and 35% respectively, doubling the residual mass for B3 reference. Both foams had lower D_s max values compared to B3 and B2 references, which indicates that they produced less amount of smoke. As the samples ignited, a char layer was formed in a couple of seconds and the flame was almost extinguished. Small flames were seen on the surface, however those ceased to exist as well, at about the 5th minute of the 10-minute testing period. Also, during the period of testing, inside of the chamber was visible, whereas during the testing of B3 and B2 foams only the silhouette of the flame was barely visible. Both samples produced LOIs about 21%. In this sense, samples with L-HNT's with much lower halogenated FR can achieve the performance of the B2 reference which contains 15 wt% halogenated FR.
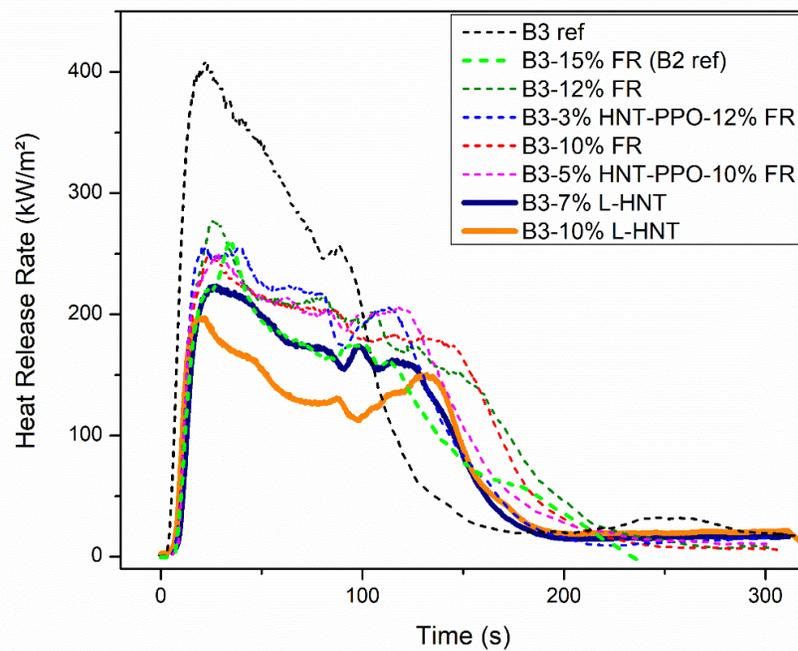
Figure 43. Heat release rate profiles of B3 foams incorporated with FR-loaded HNTs. Dotted lines are for foams containing HNT-PPO and/or FR for comparison.

Table 13. Cone calorimeter, D_s max and LOI results of B3 foams containing FR-loaded HNTs. Results for neat B3 and B2 are given for reference.

Samples	TTI (s)	pHRR (kW/m²)	THR (kW/m²)	Avg MLR (g/m²s)	Residue (%)	D_s max	LOI (%)
B3 reference	3.00±0.25	410±18	38.8±1.5	8.5±1.6	15.83±0.62	221±4	17.0
B2 ref (i.e. B3-15%FR)	6.00±1.25	267±37	27.5±0.5	10.9±3.1	28.75±1.49	231±36	22.0
B3-7%L-HNT	5.91±0.29	228±9	27.1±0.7	8.9±0.6	33.40±4.64	117±9	21.4
B3-10%L-HNT	5.58±0.38	200±24	24.4±3.9	7.4±0.7	35.51±3.64	107±10	21.0

The images of samples after the cone calorimeter test are given in Figure 44, which show char layers with some cracks. However, these layers were rigid and did not lose their integrity, but they were bent and/or separated from the polymer underneath, which may be due to the high amount of HNT added. The polymer underneath was clearly burnt, which is an indication that these char layers may have loosen their protective effects at some point. So even though the residual mass values were high for these samples, the barrier effect of the char was not pronounced. Yet, these nanocomposites with much lower halogenated FR content showed comparable results to free FR containing RPUF samples, which was presumed to be due to the slow release of FR from the HNT during the fire phenomenon. Such formulations can be further optimized to overcome the problems related to char formation mentioned above.

Figure 44. Appearance of the samples incorporated with L-HNT after testing with cone calorimeter

4.3. Conclusions

This chapter has focused on the detailed characterization of the flammability behavior of nanocomposite RPUFs with HNTs. Preliminary flame tests according to a TSE standard (TS EN ISO 11925-2) and a setup prepared in-house showed that the flames were unable to penetrate the foams. In SP foams, flame height was close to the threshold before extinguishing itself according to the small flame test. In-house flame tests showed that 10% HNT loaded sample extinguished itself in 10 seconds while for the reference it took 22 seconds for DEC foam. Yet, high amounts of smoke were observed for all these tests. Reference B3 foams not containing any FR, passed the 150 mm threshold, even in the presence of HNTs and all the samples showed similar durations to reach this limit. However, B2 foams containing FR did not reach the threshold at all and flame tests did not give any

information whether HNTs had an influence. In this sense, preliminary studies showed that detailed characterization of the flammability behavior of the nanocomposites were necessary.

Advanced characterization techniques including cone calorimeter, smoke density chamber and LOI test were used to better understand the effect of HNTs on the foams' flame retardancy behavior. HNT-PPO and FR were added to RPUFs together. Reference foam had an LOI of 17% which implies highly flammable behavior; however, addition of FR increased this value up to 22%. HNT did not significantly influence LOI. Peak heat release rates significantly decreased from about 400 kW/m^2 to 260 kW/m^2 with FR addition. With the addition of HNT-PPO, these values further decreased slightly. Average MLR values increased, which is could be attributed to the flame retardancy mechanism of the FR, which is expected to speed up the decomposition process at first, however in the end it yields higher residual mass. In terms of smoke production, both average SEA and maximum D_s values showed an increase with HNT addition. Visually, HNT addition resulted in opening of the surface char at some point during burning in cone calorimeter, probably causing penetration of flames to inside of the polymer. HNT might have disturbed the consistency of the char layer or the increased smoke production might have led to the fracture of the char due to increased pressure inside.

The incorporation of FR-loaded HNTs into foam formulations was developed as a promising approach, which resulted in quite interesting flammability behavior for RPUFs. With 7 wt% L-HNT incorporation that possessed as low as 1 wt% FR in the final foam formulation, foam's HRR behavior became comparable to that of 15 wt% free FR containing sample. 10 wt% L-HNT incorporation further improved the HRR behavior. In addition, the highest residual mass of 35% was observed at 10% L-HNT incorporation. In fact, even though L-HNT-based RPUF formulations contained much lower amount of the halogenated FR (about 1%, according to TGA results), flammability test results for foams containing L-HNTs were found to be comparable to foams with higher amounts of free FR.

Chapter 5

5. Conclusions

In this thesis, thermal insulation properties and flammability behavior of HNT reinforced RPUFs were studied. Preliminary studies showed that HNT incorporation can have a significant effect on the cell size and shape of the foams and so the thermal conductivity. The incorporation of HNTs enabled the formation of smaller cells, which positively contributed to reducing the thermal conductivity. In all studies, values below 0.040 W/m.K were obtained for the thermal conductivity of spray foam, this was reduced to about 0.025 W/m.K. However, PU foam formation is a complex reaction that is affected by many parameters. At higher HNT incorporations, some problems such as cell wall rupture and inhomogeneous cell size distribution were encountered caused by increased viscosity. High viscosity can also prevent the components from completely reacting, which would result in poor foam performance. The addition of PPO functionalized HNTs and halogenated FR into the RPUF formulation gave quite inconsistent results. Increasing FR amount in FR-only foam samples showed increased cell sizes and thermal conductivity, as expected. However, samples that had both HNT-PPO and FR were not following a trend in terms of these two properties, most probably due to poor dispersion. Nevertheless, in foams that were prepared with FR-loaded HNTs, these effects were much less pronounced compared to foams with untreated and sonicated HNTs. These foams gave more homogeneous cell size distributions and neither the morphology nor the thermal insulation properties were not negatively affected.

Preliminary testing of flammability indicated that detailed characterizations are needed, since the effects of HNT was unclear. HNT-PPO and/or halogenated FR incorporated foams were

prepared and characterized with cone calorimeter, smoke density chamber and LOI tests. The addition of FR reduced pHRR values compared to the reference, however, the addition of 3 and 5% HNT-PPO did not show any significant further reduction. FR addition also increased the MLR yet produced higher residual mass. It also greatly increased the smoke production and the smoke toxicity. Both of these can be explained by the halogenated TCPP's flame retardancy mechanism. The residual mass and smoke production increased with increasing FR amount, whereas THR values decreased. Samples that contained HNT-PPO in combination with the FR gave higher TTI, lower pHRR and THR compared to their 12 and 10% FR-only references. However, these samples also showed quite high smoke production.

Flammability tests of L-HNT incorporated foams were quite interesting. Compared to HNT-PPO and/or free FR incorporated foams, L-HNT containing RPUF samples had significantly lower pHRR and THR values along with lower smoke production. Furthermore, the thermal conductivity values of these foams continued to slightly decrease with increasing HNT, compared to the reference and remained at about 0.030 W/m.K even when considerably high amounts of HNT were added. The possible negative effect of the FR was not observed, in terms of thermal conductivity, due to the encapsulation of FT in HNTs. In fact, free FR in the foam matrix is significantly prone to volatilization and leaching, which is an environmental and health concern. Through loading this agent into the HNTs, the FR amount present in the foam formulation was substantially decreased to about 0.5-1% from the industrial standard 15%. In light of these results, foams incorporated with hybrid FR-loaded HNTs have a huge potential as flame retardant insulation materials.

References

1.   Cornille, A., et al., *A perspective approach to sustainable routes for non-isocyanate polyurethanes.* European Polymer Journal, 2017. **87**: p. 535-552.
2.   *Otto Bayer demonstrated in 1952 his invention Polyurethan.* Wikipedia.
3.   Grünbauer, H.J.M., et al., *Rigid Polyurethane Foams*, in *Polymeric Foams: Mechanisms and Materials*, S. Lee and N. Ramesh, Editors. 2004, Taylor & Francis. p. 261-318.
4.   Laoutid, F., et al., *New prospects in flame retardant polymer materials: from fundamentals to nanocomposites.* Materials Science Engineering: R: Reports, 2009. **63**(3): p. 100-125.
5.   Xu, W., G. Wang, and X. Zheng, *Research on highly flame-retardant rigid PU foams by combination of nanostructured additives and phosphorus flame retardants.* Polymer Degradation Stability, 2015. **111**: p. 142-150.
6.   Ma, W., et al., *Halloysite nanotubes: green nanomaterial for functional organic-inorganic nanohybrids.* J The Chemical Record, 2018. **18**(7-8): p. 986-999.
7.   Goda, E.S., et al., *Halloysite nanotubes as smart flame retardants: a review.* Thermochimica Acta, 2018.
8.   Santiago-Calvo, M., et al., *The effects of functional nanofillers on the reaction kinetics, microstructure, thermal and mechanical properties of water blown rigid polyurethane foams.* Polymer, 2018. **150**: p. 138-149.
9.   Singh, S.N., *Blowing Agents*, in *Handbook of Polymer Foams*, D. Eaves, Editor. 2004. p. 9-36.
10.   Eaves, D., *Rigid Polyurethane Foams*, in *Handbook of Polymer Foams*, D. Eaves, Editor. 2004. p. 55-84.
11.   Massaro, M., et al., *Chemical modification of halloysite nanotubes for controlled loading and release.* Journal of Materials Chemistry B, 2018. **6**(21): p. 3415-3433.
12.   Khobragade, P.S., et al., *Flame retarding performance of elastomeric nanocomposites: A review.* J Polymer Degradation Stability, 2016. **130**: p. 194-244.
13.   Liu, M., et al., *Recent advance in research on halloysite nanotubes-polymer nanocomposite.* J Progress in polymer science, 2014. **39**(8): p. 1498-1525.
14.   Lvov, Y., A. Aerov, and R. Fakhrullin, *Clay nanotube encapsulation for functional biocomposites.* J Advances in Colloid Interface Science, 2014. **207**: p. 189-198.
15.   Garcia-Garcia, D., et al., *Characterization of selectively etched halloysite nanotubes by acid treatment.* J Applied Surface Science, 2017. **422**: p. 616-625.
16.   Joussein, E., et al., *Halloysite clay minerals–a review.* Clay Minerals, 2005(40): p. 383-426.
17.   Melo, J.D.D., et al., *Encapsulation of solvent into halloysite nanotubes to promote self-healing ability in polymers.* J Advanced Composite Materials, 2014. **23**(5-6): p. 507-519.
18.   Rong, R., et al., *Facile preparation of homogeneous and length controllable halloysite nanotubes by ultrasonic scission and uniform viscosity centrifugation.* J Chemical Engineering Journal, 2016. **291**: p. 20-29.
19.   Lazzara, G., et al., *An assembly of organic-inorganic composites using halloysite clay nanotubes.* J Current Opinion in Colloid Interface Science, 2018. **35**: p. 42-50.
20.   Dedzo, G.K. and C. Detellier, *Clay Minerals—Ionic Liquids, Nanoarchitectures, and Applications.* J Advanced Functional Materials, 2018. **28**(27): p. 1703845.
21.   *Halloysite clay nanotubes.* [cited 2019; Available from: https://phantomplastics.com/functional-fillers/halloysite/.
22.   Cavallaro, G., G. Lazzara, and S. Milioto, *Exploiting the colloidal stability and solubilization ability of clay nanotubes/ionic surfactant hybrid nanomaterials.* J The Journal of Physical Chemistry C, 2012. **116**(41): p. 21932-21938.
23.   Zhang, A.-B., et al., *Effects of acid treatment on the physico-chemical and pore characteristics of halloysite.* J Colloids Surfaces A: Physicochemical Engineering Aspects, 2012. **396**: p. 182-188.

24. Yuan, P., D. Tan, and F. Annabi-Bergaya, *Properties and applications of halloysite nanotubes: recent research advances and future prospects.* J Applied Clay Science, 2015. **112**: p. 75-93.

25. Fu, H., et al., *Reinforcement of waterborne polyurethane with chitosan-modified halloysite nanotubes.* J Applied Surface Science, 2015. **346**: p. 372-378.

26. Jing, H., et al., *Preparation and characterization of polycarbonate nanocomposites based on surface-modified halloysite nanotubes.* Polymer Journal, 2014. **46**(5): p. 307.

27. Zheng, T. and X. Ni, *Loading an organophosphorous flame retardant into halloysite nanotubes for modifying UV-curable epoxy resin.* J RSC Advances, 2016. **6**(62): p. 57122-57130.

28. Wang, Q., et al., *Adsorption and release of ofloxacin from acid-and heat-treated halloysite.* J Colloids Surfaces B: Biointerfaces, 2014. **113**: p. 51-58.

29. Hendessi, S., et al., *Antibacterial sustained-release coatings from halloysite nanotubes/waterborne polyurethanes.* J Progress in Organic Coatings, 2016. **101**: p. 253-261.

30. Hári, J., et al., *Competitive interactions and controlled release of a natural antioxidant from halloysite nanotubes.* Journal of Colloid Interface Science, 2016. **462**: p. 123-129.

31. Kırımlıoğlu, G.Y., et al., *Gamma-aminobutyric acid loaded halloysite nanotubes and in vitro-in vivo evaluation for brain delivery.* International Journal of Pharmaceutics, 2015. **495**(2): p. 816-826.

32. Gorrasi, G., *Dispersion of halloysite loaded with natural antimicrobials into pectins: Characterization and controlled release analysis.* J Carbohydrate Polymers, 2015. **127**: p. 47-53.

33. Biddeci, G., et al., *Halloysite nanotubes loaded with peppermint essential oil as filler for functional biopolymer film.* J Carbohydrate Polymers, 2016. **152**: p. 548-557.

34. Tas, B.A., et al., *Carvacrol loaded halloysite coatings for antimicrobial food packaging applications.* Food Packaging and Shelf Life, 2019. **20**: p. 100300.

35. Fakhrullin, R., et al., *Ceramic nanotubes for polymer composites with stable anticorrosion properties.* J Crystallography Reports, 2014. **59**(7): p. 1107-1113.

36. Zahidah, K.A., et al., *Halloysite nanotubes as nanocontainer for smart coating application: A review.* J Progress in Organic Coatings, 2017. **111**: p. 175-185.

37. Abdullayev, E., et al., *Self-healing coatings based on halloysite clay polymer composites for protection of copper alloys.* J ACS Applied Materials Interfaces, 2013. **5**(10): p. 4464-4471.

38. Micó-Vicent, B., et al., *Stabilized dye–pigment formulations with platy and tubular nanoclays.* J Advanced Functional Materials, 2018. **28**(27): p. 1703553.

39. Tas, C.E., et al., *Halloysite nanotubes/polyethylene nanocomposites for active food packaging materials with ethylene scavenging and gas barrier properties.* J Food Bioprocess Technology, 2017. **10**(4): p. 789-798.

40. Gaikwad, K.K., S. Singh, and Y.S. Lee, *High adsorption of ethylene by alkali-treated halloysite nanotubes for food-packaging applications.* J Environmental Chemistry Letters, 2018: p. 1-8.

41. Massaro, M., et al., *Eco-friendly functionalization of natural halloysite clay nanotube with ionic liquids by microwave irradiation for Suzuki coupling reaction.* Journal of Organometallic Chemistry, 2014. **749**: p. 410-415.

42. K. Dedzo, G., G.l. Ngnie, and C. Detellier, *PdNP decoration of halloysite lumen via selective grafting of ionic liquid onto the aluminol surfaces and catalytic application.* ACS Applied Materials Interfaces, 2016. **8**(7): p. 4862-4869.

43. Luo, P., et al., *Study on the adsorption of Neutral Red from aqueous solution onto halloysite nanotubes.* J Water Research, 2010. **44**(5): p. 1489-1497.

44.   Jinhua, W., et al., *Rapid adsorption of Cr (VI) on modified halloysite nanotubes.* J Desalination, 2010. **259**(1-3): p. 22-28.

45.   Liu, R., et al., *Adsorption of methyl violet from aqueous solution by halloysite nanotubes.* J Desalination, 2011. **268**(1-3): p. 111-116.

46.   Bonifacio, M.A., et al., *Insight into halloysite nanotubes-loaded gellan gum hydrogels for soft tissue engineering applications.* J Carbohydrate Polymers, 2017. **163**: p. 280-291.

47.   Ji, L., et al., *A gelatin composite scaffold strengthened by drug-loaded halloysite nanotubes.* J Materials Science Engineering: C, 2017. **78**: p. 362-369.

48.   Ana, C.S., et al., *Halloysite clay nanotubes for life sciences applications: from drug encapsulation to bioscaffold.* J Advances in Colloid Interface Science, 2018.

49.   Maubru, M., S. Restle, and B. Perron, *Cosmetic compositions comprising a methacrylic acid copolymer, insoluble mineral particles and a cationic or amphoteric polymers.* 2004, Industrial report, L'oreal, France.

50.   Ha, S. and H. Lee, *Cosmetic composition for preventing the skin aging and whitening the skin, containing natural mixture having plentiful inorganic substances including selenium.* 2003, Industrial report, Korea Research Institute of Chemical Technology, South Korea.

51.   Wilson, I., *Kaolin and halloysite deposits of China.* Clay Minerals, 2004. **39**(1): p. 1-15.

52.   Pandey, G., D. Rawtani, and Y. Agrawal, *Future Aspects of Halloysite Nanotubes in Forensic Investigations.* Journal of Nanomedicine Research, 2017. **6**(2): p. 2.

53.   Sun, P., et al., *Effective activation of halloysite nanotubes by piranha solution for amine modification via silane coupling chemistry.* RSC Advances, 2015. **5**(65): p. 52916-52925.

54.   Frank, B.P., et al., *Impact of Silanization on the Structure, Dispersion Properties, and Biodegradability of Nanocellulose as a Nanocomposite Filler.* ACS Applied Nano Materials, 2018. **1**(12): p. 7025-7038.

55.   Saif, M.J., H.M. Asif, and M. Naveed, *PROPERTIES AND MODIFICATION METHODS OF HALLOYSITE NANOTUBES: A STATE-OF-THE-ART REVIEW.* Journal of the Chilean Chemical Society, 2018. **63**(3): p. 4109-4125.

56.   Lee, L.J., et al., *Polymer nanocomposite foams.* Composites science technology, 2005. **65**(15-16): p. 2344-2363.

57.   Raman, V., et al., *Reinforcement of solution styrene butadiene rubber by silane functionalized halloysite nanotubes.* Journal of Macromolecular Science, Part A, 2013. **50**(11): p. 1091-1106.

58.   Rong, R., et al., *Facile preparation of homogeneous and length controllable halloysite nanotubes by ultrasonic scission and uniform viscosity centrifugation.* Chemical Engineering Journal, 2016. **291**: p. 20-29.

59.   Tharmavaram, M., G. Pandey, and D. Rawtani, *Surface modified halloysite nanotubes: A flexible interface for biological, environmental and catalytic applications.* Advances in Colloid Interface Science, 2018.

60.   Rimsza, J.M., R.E. Jones, and L.J. Criscenti, *Interaction of NaOH solutions with silica surfaces.* Journal of Colloid Interface Science, 2018. **516**: p. 128-137.

61.   Li, C., et al., *A general synthesis approach toward halloysite-based composite nanotube.* Journal of Applied Polymer Science, 2009. **112**(5): p. 2647-2655.

62.   Yuan, P., et al., *Functionalization of halloysite clay nanotubes by grafting with γ-aminopropyltriethoxysilane.* The Journal of Physical Chemistry C, 2008. **112**(40): p. 15742-15751.

63.   Joo, Y., et al., *Opening and blocking the inner-pores of halloysite.* Chemical Communications, 2013. **49**(40): p. 4519-4521.

64.   Wang, Q., J. Zhang, and A. Wang, *Alkali activation of halloysite for adsorption and release of ofloxacin.* Applied Surface Science, 2013. **287**: p. 54-61.

65.   Vogel, B.M., et al., *Interfacial modification of silica surfaces through γ-isocyanatopropyl triethoxy silane–amine coupling reactions.* Applied Surface Science, 2008. **254**(6): p. 1789-1796.

66.   Yuan, P., et al., *Organosilane functionalization of halloysite nanotubes for enhanced loading and controlled release.* Nanotechnology, 2012. **23**(37): p. 375705.

67.   Yah, W.O., A. Takahara, and Y.M. Lvov, *Selective modification of halloysite lumen with octadecylphosphonic acid: new inorganic tubular micelle.* Journal of the American Chemical Society, 2012. **134**(3): p. 1853-1859.

68.   Tang, Y., et al., *Effects of unfolded and intercalated halloysites on mechanical properties of halloysite–epoxy nanocomposites.* Composites Part A: Applied Science Manufacturing, 2011. **42**(4): p. 345-354.

69.   Lvov, Y., et al., *Thin film nanofabrication via layer-by-layer adsorption of tubule halloysite, spherical silica, proteins and polycations.* Colloids Surfaces A: Physicochemical Engineering Aspects, 2002. **198**: p. 375-382.

70.   Yah, W.O., et al., *Biomimetic dopamine derivative for selective polymer modification of halloysite nanotube lumen.* Journal of the American Chemical Society, 2012. **134**(29): p. 12134-12137.

71.   Shamsi, M.H. and K.E. Geckeler, *The first biopolymer-wrapped non-carbon nanotubes.* Nanotechnology, 2008. **19**(7): p. 075604.

72.   Zainuddin, S., et al., *Morphological and mechanical behavior of chemically treated jute-PHBV bio-nanocomposites reinforced with silane grafted halloysite nanotubes.* Journal of Applied Polymer Science, 2016. **133**(39).

73.   Yaghoubi, A. and M.M.A. Nikje, *Silanization of multi-walled carbon nanotubes and the study of its effects on the properties of polyurethane rigid foam nanocomposites.* Composites Part A: Applied Science Manufacturing, 2018. **109**: p. 338-344.

74.   Rapacz-Kmita, A., et al., *Functionalized halloysite nanotubes as a novel efficient carrier for gentamicin.* Materials Letters, 2019. **243**: p. 13-16.

75.   Bischoff, E., et al., *Organosilane-functionalized halloysite for high performance halloysite/heterophasic ethylene–propylene copolymer nanocomposites.* Applied Clay Science, 2015. **112**: p. 68-74.

76.   Terzopoulou, Z., et al., *Effect of surface functionalization of halloysite nanotubes on synthesis and thermal properties of poly (ε-caprolactone).* Journal of materials science, 2018. **53**(9): p. 6519-6541.

77.   Peixoto, A.F., et al., *Physicochemical characterization of organosilylated halloysite clay nanotubes.* Microporous Mesoporous Materials, 2016. **219**: p. 145-154.

78.   Yuan, P., et al., *Changes in structure, morphology, porosity, and surface activity of mesoporous halloysite nanotubes under heating.* Clays Clay Minerals, 2012. **60**(6): p. 561-573.

79.   Mouritz, A.P. and A.G. Gibson, *Fire tests for composites*, in *Fire properties of polymer composite materials*. 2007, Springer Science & Business Media. p. 325-358.

80.   Thirumal, M., et al., *Effect of a nanoclay on the mechanical, thermal and flame retardant properties of rigid polyurethane foam.* Journal of Macromolecular Science, Part A: Pure Applied Chemistry, 2009. **46**(7): p. 704-712.

81.   Yang, R., et al., *Synthesis, mechanical properties and fire behaviors of rigid polyurethane foam with a reactive flame retardant containing phosphazene and phosphate.* Polymer Degradation Stability, 2015. **122**: p. 102-109.

82.   Qi, X., et al., *Thermal, mechanical, and morphological properties of rigid crude glycerol-based polyurethane foams reinforced with nanoclay and microcrystalline cellulose.* European journal of lipid science technology, 2018. **120**(5): p. 1700413.

83. Saha, M., M.E. Kabir, and S. Jeelani, *Enhancement in thermal and mechanical properties of polyurethane foam infused with nanoparticles.* Materials Science Engineering: A, 2008. **479**(1-2): p. 213-222.

84. Lorusso, C., et al., *Thermal and mechanical performance of rigid polyurethane foam added with commercial nanoparticles.* Nanomaterials Nanotechnology, 2017. **7**: p. 1847980416684117.

85. Chen, Y., et al., *Preparation of polymeric foams with bimodal cell size: An application of heterogeneous nucleation effect of nanofillers.* The Journal of Supercritical Fluids, 2019. **147**: p. 107-115.

86. Pethrick, R.A., *Fire-Retarded Environmentally Friendly Flexible Foam Materials Using Nanotechnology*, in *Environanotechnology*. 2010, Elsevier. p. 213-220.

87. Kang, J.W., et al., *Effects of nucleating agents on the morphological, mechanical and thermal insulating properties of rigid polyurethane poams.* Macromolecular Research, 2009. **17**(11): p. 856-862.

88. Estravís, S., et al., *Rigid polyurethane foams with infused nanoclays: relationship between cellular structure and thermal conductivity.* European Polymer Journal, 2016. **80**: p. 1-15.

89. Qi, X., et al., *Thermal, mechanical, and morphological properties of rigid crude glycerol-based polyurethane foams reinforced with nanoclay and microcrystalline cellulose.* European Journal of Lipid Science and Technology, 2018. **120**(5): p. 1700413.

90. Glicksman, L.R., *Heat transfer in foams*, in *Low density cellular plastics*. 1994, Springer. p. 104-152.

91. Biedermann, A., et al., *Analysis of heat transfer mechanisms in polyurethane rigid foam.* Journal of Cellular Plastics, 2001. **37**(6): p. 467-483.

92. Stazi, F., et al., *Thermal and mechanical optimization of nano-foams for sprayed insulation.* Construction Building Materials, 2019. **201**: p. 828-841.

93. Ferkl, P., et al., *Multi-scale modelling of heat transfer in polyurethane foams.* Chemical Engineering Science, 2017. **172**: p. 323-334.

94. Ahern, A., et al., *The conductivity of foams: a generalisation of the electrical to the thermal case.* Colloids Surfaces A: Physicochemical Engineering Aspects, 2005. **263**(1-3): p. 275-279.

95. Reitz, D., M. Schuetz, and L. Glicksman, *A basic study of aging of foam insulation.* Journal of Cellular Plastics, 1984. **20**(2): p. 104-113.

96. Nielsen, L.V., et al., *Thermal conductivity of nonporous polyurethane.* High Temperatures High Pressures, 2000. **32**(6): p. 701-707.

97. Schuetz, M. and L.R. Glicksman, *A basic study of heat transfer through foam insulation.* Journal of Cellular Plastics, 1984. **20**(2): p. 114-121.

98. Glicksman, L., M. Schuetz, and M. Sinofsky, *Radiation heat transfer in foam insulation.* International Journal of Heat Mass Transfer, 1987. **30**(1): p. 187-197.

99. Fang, W., et al., *Numerical predictions of the effective thermal conductivity of the rigid polyurethane foam.* Journal of Wuhan University of Technology-Mater. Sci. Ed., 2017. **32**(3): p. 703-708.

100. Lee, S.-T., C.B. Park, and N.S. Ramesh, *Relationships Between Foam Structure and Properties*, in *Polymeric foams: science and technology*. 2006, CRC press. p. 93-116.

101. Hoogendoorn, C.J., *Thermal aging*, in *Low density cellular plastics*. 1994, Springer. p. 153-186.

102. Wassiljewa, A., *Warmeleitung in gasgemischen.* Physik. Z., 1904. **5**: p. 737-742.

103. Lindsay, A.L. and L.A. Bromley, *Thermal conductivity of gas mixtures.* Industrial Engineering Chemistry, 1950. **42**(8): p. 1508-1511.

104. Jarfelt, U. and O. Ramnäs. *Thermal conductivity of polyurethane foam-best performance*. in *10th International Symposium on district heating and cooling*. 2006. Chalmers University of Technology Goteborg, Sweden.

105. Choe, H., Y. Choi, and J.H. Kim, *Threshold cell diameter for high thermal insulation of water-blown rigid polyurethane foams.* Journal of Industrial Engineering Chemistry, 2019. **73**: p. 344-350.

106. Coquard, R., D. Baillis, and J. Randrianalisoa, *Homogeneous phase and multi-phase approaches for modeling radiative transfer in foams.* International Journal of Thermal Sciences, 2011. **50**(9): p. 1648-1663.

107. Luo, P., et al., *Preparation and characterization of silane coupling agent modified halloysite for Cr (VI) removal.* Industrial Engineering Chemistry Research, 2011. **50**(17): p. 10246-10252.

108. Zhu, K., et al., *Silane-modified halloysite/Fe3O4 nanocomposites: simultaneous removal of Cr (VI) and Sb (V) and positive effects of Cr (VI) on Sb (V) adsorption.* Chemical Engineering Journal, 2017. **311**: p. 236-246.

109. Singh, H., A. Jain, and T. Sharma, *Effect of phosphorus-nitrogen additives on fire retardancy of rigid polyurethane foams.* Journal of Applied Polymer Science, 2008. **109**(4): p. 2718-2728.

110. Yang, H., et al., *Diphase flame-retardant effect of ammonium polyphosphate and dimethyl methyl phosphonate on polyisocyanurate-polyurethane foam.* Polymers for Advanced Technologies, 2018. **29**(12): p. 2917-2925.

111. Wang, K., A.B. Morgan, and V. Benin, *Preparation and studies of new phosphorus-containing diols as potential flame retardants.* Fire Materials, 2017. **41**(8): p. 973-982.

112. Vini, R., S. Thenmozhi, and S. Murugavel, *Synthesis, characterization and thermal degradation kinetics of azomethine-based halogen-free flame-retardant polyphosphonates.* High Performance Polymers, 2019. **31**(1): p. 86-96.

113. Szczotok, A., et al. *Development of thermoregulating microcapsules with cyclotriphosphazene as a flame retardant agent.* in *IOP Conference Series: Materials Science and Engineering.* 2017. IOP Publishing.

114. Liu, W., R.J. Varley, and G.P. Simon, *A phosphorus-containing diamine for flame-retardant, high-functionality epoxy resins. I. Synthesis, reactivity, and thermal degradation properties.* Journal of Applied Polymer Science, 2004. **92**(4): p. 2093-2100.

115. Kuo, P.L., J.M. Chang, and T.L. Wang, *Flame-retarding materials—I. Syntheses and flame-retarding property of alkylphosphate-type polyols and corresponding polyurethanes.* Journal of Applied Polymer Science, 1998. **69**(8): p. 1635-1643.

116. Palacios, A., et al., *Study of the thermal properties and the fire performance of flame retardant-organic PCM in bulk form.* Materials, 2018. **11**(1): p. 117.

117. DOT/FAA/AR-05/14, O.o.A.R., *Polymer flammability.* 2005: Washington, D.C. 20591.

118. Daniel, Y.G. and B.A. Howell, *Flame retardant properties of isosorbide bis-phosphorus esters.* Polymer Degradation Stability, 2017. **140**: p. 25-31.

119. Ye, L., et al., *Flame-retardant and mechanical properties of high-density rigid polyurethane foams filled with decabrominated dipheny ethane and expandable graphite.* Journal of Applied Polymer Science, 2009. **111**(5): p. 2372-2380.

120. Lecouvet, B., et al., *A comprehensive study of the synergistic flame retardant mechanisms of halloysite in intumescent polypropylene.* Polymer Degradation Stability, 2013. **98**(11): p. 2268-2281.

121. Żabski, L., W. Walczyk, and D. Weleda, *Flammability and thermal properties of rigid polyurethane foams with additionally introduced cyclic structures.* Journal of Applied Polymer Science, 1980. **25**(12): p. 2659-2680.

122. Thirumal, M., et al., *Halogen-free flame retardant PUF: effect of melamine compounds on mechanical, thermal and flame retardant properties.* Polymer Degradation Stability, 2010. **95**(6): p. 1138-1145.

123. Rybiński, P. and G. Janowska, *Influence synergetic effect of halloysite nanotubes and halogen-free flame-retardants on properties nitrile rubber composites.* Thermochimica Acta, 2013. **557**: p. 24-30.

124. Sivriev, C. and L. Żabski, *Flame retarded rigid polyurethane foams by chemical modification with phosphorus-and nitrogen-containing polyols.* European Polymer Journal, 1994. **30**(4): p. 509-514.

125. Schmitt, E., *Phosphorus-based flame retardants for thermoplastics.* Plastics, Additives Compounding, 2007. **9**(3): p. 26-30.

126. Hörold, S., *Phosphorus-based and intumescent flame retardants*, in *Polymer Green Flame Retardants.* 2014, Elsevier. p. 221-254.

127. Liang, S., et al., *Flame retardancy and thermal decomposition of flexible polyurethane foams: Structural influence of organophosphorus compounds.* Polymer Degradation Stability, 2012. **97**(11): p. 2428-2440.

128. Meng, X.Y., et al., *Effects of expandable graphite and ammonium polyphosphate on the flame-retardant and mechanical properties of rigid polyurethane foams.* Journal of Applied Polymer Science, 2009. **114**(2): p. 853-863.

129. Ren, X., et al., *A novel application of phosphorene as a flame retardant.* Polymers, 2018. **10**(3): p. 227.

130. Alongi, J., Z. Han, and S. Bourbigot, *Intumescence: tradition versus novelty. A comprehensive review.* Progress in Polymer Science, 2015. **51**: p. 28-73.

131. Bourbigot, S. and S. Duquesne, *Fire retardant polymers: recent developments and opportunities.* Journal of Materials Chemistry, 2007. **17**(22): p. 2283-2300.

132. Gao, S., X. Zhao, and G. Liu, *Synthesis of an integrated intumescent flame retardant and its flame retardancy properties for polypropylene.* Polymer Degradation Stability, 2017. **138**: p. 106-114.

133. Wang, W., et al., *Synthesis of a novel charring agent containing pentaerythritol and triazine structure and its intumescent flame retardant performance for polypropylene.* Polymer Degradation Stability, 2017. **144**: p. 454-463.

134. Sittisart, P. and M.M. Farid, *Fire retardants for phase change materials.* J Applied Energy, 2011. **88**(9): p. 3140-3145.

135. Xu, D., K. Yu, and K. Qian, *Effect of tris (1-chloro-2-propyl) phosphate and modified aramid fiber on cellular structure, thermal stability and flammability of rigid polyurethane foams.* Polymer Degradation Stability, 2017. **144**: p. 207-220.

136. Gaan, S., et al., *Effect of nitrogen additives on flame retardant action of tributyl phosphate: phosphorus–nitrogen synergism.* Polymer Degradation Stability, 2008. **93**(1): p. 99-108.

137. Rao, W.-H., et al., *Flame-retardant flexible polyurethane foams with highly efficient melamine salt.* Industrial Engineering Chemistry Research, 2017. **56**(25): p. 7112-7119.

138. Zhang, M., et al., *Effects of a novel phosphorus–nitrogen flame retardant on rosin-based rigid polyurethane foams.* Polymer Degradation Stability, 2015. **120**: p. 427-434.

139. Truong, J.W., et al., *Isomers of tris (chloropropyl) phosphate (TCPP) in technical mixtures and environmental samples.* Analytical Bioanalytical Chemistry, 2017. **409**(30): p. 6989-6997.

140. Antonopoulou, M., et al., *Degradation of organophosphorus flame retardant tris (1-chloro-2-propyl) phosphate (TCPP) by visible light N, S-codoped TiO2 photocatalysts.* Chemical Engineering Journal, 2017. **318**: p. 231-239.

141. Denecker, C., J. Liggat, and C. Snape, *Relationship between the thermal degradation chemistry and flammability of commercial flexible polyurethane foams.* Journal of Applied Polymer Science, 2006. **100**(4): p. 3024-3033.

142. Skibińska, M., *The sorption capability of halloysite.* Annales Universitatis Mariae Curie-Sklodowska, sectio AA–Chemia, 2017. **72**(1): p. 47.

143.   Gillani, Q., et al., *A synergy study of zinc borate in halloysite nanotube reinforced, siloxane epoxy base intumescent fire resistive coatings: Eine Synergieuntersuchung zu Zinkborat in, mit Halloysit-Nanoröhren verstärkten, Siloxane Epoxy basierten, intumeszenten feuerfesten Beschichtungen.* Materialwissenschaft und Werkstofftechnik, 2018. **49**(4): p. 420-426.

144.   Zheng, X., G. Wang, and W. Xu, *Roles of organically-modified montmorillonite and phosphorous flame retardant during the combustion of rigid polyurethane foam.* Polymer Degradation Stability, 2014. **101**: p. 32-39.

145.   Jia, Z., et al., *Reinforcing and flame-retardant effects of halloysite nanotubes on LLDPE.* Polymer-Plastics Technology Engineering, 2009. **48**(6): p. 607-613.

146.   Lecouvet, B., et al., *Thermal and flammability properties of polyethersulfone/halloysite nanocomposites prepared by melt compounding.* Polymer Degradation Stability, 2013. **98**(10): p. 1993-2004.

147.   Liu, C., et al., *Thermal degradation behaviors of poly (vinyl chloride)/halloysite nanotubes nanocomposites.* International Journal of Polymeric Materials, 2013. **62**(3): p. 128-132.

148.   Kenig, S., *Nanoclays containing flame retardant chemicals for fire retardant applications.* 2016, Google Patents.

149.   Du, M., B. Guo, and D. Jia, *Thermal stability and flame retardant effects of halloysite nanotubes on poly (propylene).* European Polymer Journal, 2006. **42**(6): p. 1362-1369.

150.   Sahnoune, M., et al., *Fire retardancy effect of phosphorus-modified halloysite on polyamide-11 nanocomposites.* Polymer Engineering Science, 2019. **59**(3): p. 526-534.

151.   Vahabi, H., et al., *Flame retardant epoxy/halloysite nanotubes nanocomposite coatings: exploring low-concentration threshold for flammability compared to expandable graphite as superior fire retardant.* Progress in Organic Coatings, 2018. **119**: p. 8-14.

152.   Marney, D., et al., *The suitability of halloysite nanotubes as a fire retardant for nylon 6.* Polymer Degradation Stability, 2008. **93**(10): p. 1971-1978.

153.   da Silva Ribeiro, S.P., et al., *Effect of clay minerals structure on the polymer flame retardancy intumescent process.* Applied Clay Science, 2018. **161**: p. 301-309.

154.   Wang, Y., et al., *Synergistic effect of halloysite nanotubes on flame resistance of intumescent flame retardant poly (butylene succinate) composites.* Polymer Composites, 2019.

155.   Joshi, A.R., et al., *Enhanced flame retardancy of latex coating doped with clay nanotubes.* Journal of Coatings Technology Research, 2016. **13**(3): p. 535-541.

156.   Jing, H., et al., *Internally modified halloysite nanotubes as inorganic nanocontainers for a flame retardant.* Chemistry Letters, 2013. **42**(2): p. 121-123.

157.   Marney, D., et al., *Phosphorus intercalation of halloysite nanotubes for enhanced fire properties of polyamide 6.* 2012. **23**(12): p. 1564-1571.

158.   Zheng, T. and X. Ni, *Loading an organophosphorous flame retardant into halloysite nanotubes for modifying UV-curable epoxy resin.* RSC Advances, 2016. **6**(62): p. 57122-57130.

159.   Boonkongkaew, M. and K. Sirisinha, *Halloysite nanotubes loaded with liquid organophosphate for enhanced flame retardancy and mechanical properties of polyamide 6.* Journal of materials science, 2018. **53**(14): p. 10181-10193.

160.   Smith, R.J., et al., *Environmentally benign halloysite nanotube multilayer assembly significantly reduces polyurethane flammability.* Advanced Functional Materials, 2018. **28**(27): p. 1703289.